

See discussions, stats, and author profiles for this publication at: <https://www.researchgate.net/publication/271332510>

# New Look at Hemoglobin Allostery

ARTICLE *in* CHEMICAL REVIEWS · JANUARY 2015

Impact Factor: 46.57 · DOI: 10.1021/cr500495x · Source: PubMed

---

CITATIONS

7

READS

35

---

## 4 AUTHORS, INCLUDING:



[Yue Yuan](#)

University of Notre Dame

19 PUBLICATIONS 490 CITATIONS

[SEE PROFILE](#)



[Virgil Simplaceanu](#)

Carnegie Mellon University

91 PUBLICATIONS 1,607 CITATIONS

[SEE PROFILE](#)



[Chien Ho](#)

Carnegie Mellon University

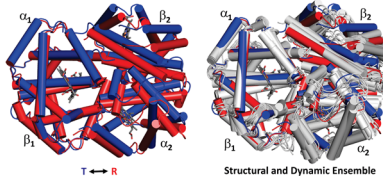
377 PUBLICATIONS 9,305 CITATIONS

[SEE PROFILE](#)

## New Look at Hemoglobin Allostery

<sup>1</sup> Yue Yuan, Ming F. Tam, Virgil Simplaceanu, and Chien Ho\*

<sup>2</sup> Department of Biological Sciences, Carnegie Mellon University, Pittsburgh, Pennsylvania 15213, United States



### CONTENTS

- <sup>7</sup> 1. Introduction
- <sup>8</sup> 2. Structure
  - <sup>9</sup> 2.1. Crystal Structures of Hemoglobin Determined by X-ray Crystallography
  - <sup>10</sup> 2.2. Solution Structures of Hemoglobin and Effects of Inositol Hexaphosphate Investigated by NMR
    - <sup>11</sup> 2.2.1. Quaternary Structures of HbCO A and Deoxy-Hb A in Solution
    - <sup>12</sup> 2.2.2. Solution Structure of HbCO A and Effects of IHP
  - <sup>13</sup> 2.3. Wide-Angle X-ray Scattering Investigation of Hemoglobin Structures in Solution
- <sup>20</sup> 3. Dynamics
  - <sup>21</sup> 3.1. Backbone Dynamics Analyzed by <sup>15</sup>N Relaxation Parameters
  - <sup>23</sup> 3.2. Dynamics of Tryptophan Residues Analyzed by <sup>15</sup>N Relaxation Parameters
  - <sup>25</sup> 3.3. Dynamics of Methyl Groups Analyzed by <sup>13</sup>C Relaxation Parameters
  - <sup>27</sup> 3.4. Amide–Water Exchange Measured by NMR
- <sup>28</sup> 4. Function
  - <sup>29</sup> 4.1. Effects of Hydrogen Ions and Allosteric Effectors on Oxygen Affinity
  - <sup>31</sup> 4.2. Effect of Temperature on Oxygen Affinity
  - <sup>32</sup> 4.3. Oxygen Affinity Related to the Distal Hydrogen Bond
  - <sup>34</sup> 4.4. Autoxidation
  - <sup>35</sup> 4.5. Effects of Interfacial and Distal Heme-Pocket Mutations on the Structure and Function of Hemoglobin
- <sup>38</sup> 5. Dynamic and Structural Basis of Hemoglobin Allostery
- <sup>39</sup> 6. Concluding Remarks
- <sup>41</sup> Author Information
  - <sup>42</sup> Corresponding Author
  - <sup>43</sup> Notes
  - <sup>44</sup> Biographies
  - <sup>45</sup> Acknowledgments
  - <sup>46</sup> Abbreviations
  - <sup>47</sup> References

### 1. INTRODUCTION

Hemoglobin (Hb) is a truly remarkable molecule. Human adult hemoglobin (Hb A) has a tetrameric structure consisting of two  $\alpha$ -chains with 141 amino acids each and two  $\beta$ -chains with 146 amino acids each. Figure 1 illustrates features of the molecule that will be discussed. The tertiary structure is the three-dimensional structure of the individual protein chains. The quaternary structure is the arrangement of the multiple protein chains into a multisubunit complex stabilized through non-covalent interactions. Each of the four chains in Hb possesses a heme group, the binding site for ligands, such as oxygen ( $O_2$ ), carbon monoxide (CO), or nitric oxide (NO). It is an essential protein for all vertebrates, designed to facilitate the loading of oxygen molecules in the lungs (or gills) and unloading of oxygen molecules in the tissues efficiently. Hb is one of the first proteins whose structure was determined by X-ray crystallography in the 1960s and has also been used as a paradigm for understanding the structure–function relationship in allosteric proteins. An allosteric protein is one in which binding of a substrate, product, or other effector to a subunit of a multisubunit protein at a site (allosteric site) other than the functional site alters its conformation and functional properties and can therefore contribute to regulating its physiological properties. For a review of the structure–function relationship of Hb, see ref 1. Most of the published results and conclusions regarding the molecular basis for Hb function, until recently, were based on the information derived from X-ray crystallographic data of Hb, e.g., the classical Monod–Wyman–Changeux (MWC) and Perutz’s two-structure stereochemical model for hemoglobin allostery.<sup>2,3</sup>

The classical MWC/Perutz model postulates that all four subunits in Hb have to assume simultaneously either the tense (T) or the relaxed (R) structure.<sup>2,3</sup> Both structures can bind ligands, while the affinity toward the ligand changes in transiting from the T to the R structure. Noticing the marked differences in the crystal structures of oxy- and deoxy-Hb, Perutz<sup>3</sup> put forward his stereochemical mechanism that correlated the T and R states of the MWC model to the deoxy and oxy structures of Hb. A key feature of the MWC model is that all four subunits must make the switch from T to R or R to T at the same time. In other words, the ligation of one subunit would not affect the ligand affinity of the neighboring subunits within the same quaternary structure. It is a concerted quaternary structural transition model. Perutz’s model further postulates that inter- and intrasubunit salt bridges stabilize the Hb molecule in the T structure. The deoxy or T structure has a lower ligand affinity compared to the oxy or R structure, and the binding of oxygen is cooperative, i.e.,

Received: September 3, 2014

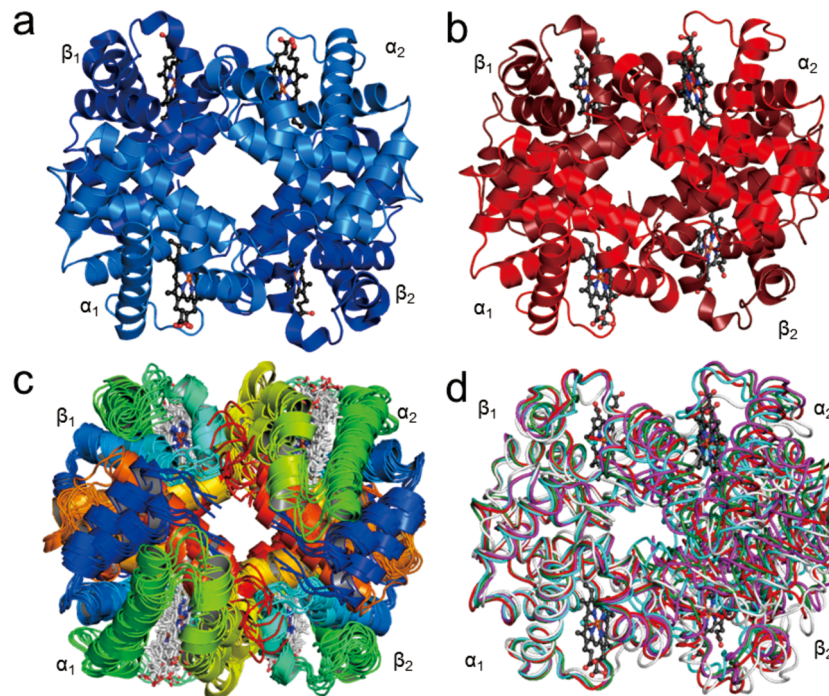


**Figure 1.** Structures of Hb A: (a) Crystal structure of deoxy-Hb A (2DN2); (b) crystal structure of HbCO A (2DN3); (c) 10 lowest energy solution structures of HbCO A obtained by NMR spectroscopy (2M6Z); (d) superimposition of the R (2DN3, red), R2 (1BBB, magenta), RR2 (1MKO, green), and R3 (1YZI, cyan) crystal structures of HbCO A with the average solution structure obtained by NMR (light gray). Structures are aligned according to the  $\alpha_1\beta_1$  dimer. Figures were generated with the PyMOL program.<sup>61</sup>

95 binding of the first oxygen molecule increases the affinity of the  
96 Hb molecule for additional oxygen molecules.

97 The induced-fit or sequential model [also known as the  
98 Koshland–Nemethy–Filmer (KNF) model] is another classical  
99 model for Hb allostericity.<sup>4,5</sup> It postulates that the binding of a  
100 ligand to one subunit can induce the conformational changes in  
101 the tertiary structure of its neighboring subunits without their  
102 having a bound ligand. Thus, the ligand binding in a  
103 multisubunit protein is a sequential process; there are not  
104 just two final states, T and R, but a series of intermediate states.  
105 A conformational change in a neighboring subunit can take  
106 place in the absence of ligand binding.

107 Both the MWC and the KNF models can account for the  
108 cooperative oxygen binding to Hb; thus, the ligand-binding  
109 data alone cannot distinguish the KNF model from the MWC/  
110 Perutz model. Much work has been done in the last 60 years in  
111 order to determine whether the transition from the T to the R  
112 state is concerted or sequential and to gain an understanding of  
113 the atomic and molecular details of the cooperative oxygenation  
114 of Hb A and the mechanism of allosterity.

115 The stereochemical mechanism of Perutz was extended by  
116 Szabo and Karplus<sup>6</sup> and later refined by Lee and Karplus.<sup>7</sup> This  
117 statistical-mechanical model derives a partition function that  
118 describes the influence of homotropic (oxygen) and hetero-  
119 tropic [e.g., hydrogen ions and 2,3-bisphosphoglycerate (2,3-  
120 BPG)] effectors on the Hb structural changes. Two different  
121 tertiary structures for each of the two quaternary structures  
122 have been included in their formulation. Contrary to Perutz's  
123 model, the Szabo–Karplus model takes into account the  
124 differences in strength of the salt bridges that stabilize the T  
125 structure and the contributions of the pH-independent steric  
126 constraints in reducing the ligand affinity of Hb in the deoxy  
127 state.

Yonetani and co-workers proposed a global allosteric model.<sup>8</sup> This model stipulates that in the absence of heterotropic effectors, the allosteric of Hb follows the MWC/Perutz model. Heterotropic effectors, when present, interact with both T and R states of Hb to induce tertiary rather than quaternary structural changes. The changes in oxygen affinity, Bohr effect, and cooperativity of Hb are primarily the consequence of heterotropic effector-induced tertiary structural changes.

The tertiary two-state model of Eaton and co-workers<sup>9</sup> can be considered as a variation of the MWC/Perutz model. Within each quaternary structure, the subunits exist in equilibrium of high (*r*) and low (*t*) affinity conformers. The R and T structures as defined in the MWC/Perutz model favor the *r* and *t* formation, respectively. As in the MWC/Perutz model, ligand binding without a quaternary conformation change is non-cooperative. However, the tertiary conformations of individual subunits play the primary role instead of the quaternary conformations.

The molecular code for cooperativity of Ackers and co-workers<sup>10,11</sup> points out that there are eight ligation intermediates between the completely unliganded and the fully liganded tetrameric Hb. The tetrameric Hb switches from T to R form when at least one subunit of each dimer is liganded. Hence, five ligation intermediates plus the fully liganded tetrameric Hb exist in the R structure. Within each quaternary state, oxygen binding or releasing “sequentially” modulates the tertiary constraints, which ultimately leads to the quaternary structural switch. Cooperativity is the result of both “concerted” quaternary switching and “sequential” modulation of ligand binding within each quaternary form.

There are many crystal structures determined over the years, and several well-characterized T and R types of crystal structures of Hb A reported in the literature are summarized in Table 1. This multitude of structures and recent results

**Table 1.** Crystallization Conditions and Resolutions of Various Crystal Structures

PDB code	resolution (Å)	space group	R factor	ligation state/ ligand	experimental condition			
					crystallization buffer	pH	T (°C)	ref
1HHO	2.10	P4 <sub>1</sub> 2 <sub>1</sub> 2	0.223	R/O <sub>2</sub>	2.25–3.0 M phosphate	6.8–8.5	4	45
1BBB <sup>a</sup>	1.70	P2 <sub>1</sub> 2 <sub>1</sub> 2 <sub>1</sub>	0.184	R2/CO	100 mM (CH <sub>3</sub> ) <sub>2</sub> AsO <sub>2</sub> Na, 75 mM HCl and 16% PEG 6000	5.8	rt	47
1MKO <sup>a,b</sup>	2.18	P2 <sub>1</sub> 2 <sub>1</sub> 2 <sub>1</sub>	0.200	RR2/CO	2.25–2.75 M phosphate	6.7	rt	53
1YZI <sup>b</sup>	2.07	P4 <sub>1</sub> 2 <sub>2</sub>	0.208	R3/CO		7.1		
2DN1 <sup>b</sup>	1.25	P4 <sub>1</sub> 2 <sub>1</sub> 2	0.195	R/O <sub>2</sub>	2.4 M phosphate, 10% glycerol	6.7	4	35
2DN3 <sup>b</sup> (1IRD <sup>a</sup> )	1.25	P4 <sub>1</sub> 2 <sub>1</sub> 2	0.183	R/CO			20	
1LJW <sup>b</sup>	2.16	P4 <sub>1</sub> 2 <sub>1</sub> 2	0.205	R/CO	2.35–2.65 M phosphate	6.4	rt	44
3HXN	2.00	P2 <sub>1</sub>	0.225	R/IHP, CO				
4N7N	2.75	C2	0.251	R <sub>mix</sub> /met	10 mM KH <sub>2</sub> PO <sub>4</sub> , 18% PEG3350 and 5% glycerol	6.8	20	60
4HHB <sup>a</sup>	1.74	P2 <sub>1</sub>	0.135	T/deoxy	3.6 M ammonium sulfate/phosphate	6.5	rt	42
2DN2 <sup>a</sup>	1.25	P2 <sub>1</sub>	0.179	T/deoxy	3.6 M ammonium sulfate/phosphate	6.5	20	35
1A3N <sup>a,b</sup>	1.80	P2 <sub>1</sub>	0.171	T/deoxy	3.6 M ammonium sulfate/phosphate	6.5	rt	46
1HGA <sup>a</sup>	2.10	P2 <sub>1</sub> 2 <sub>1</sub> 2	0.200	T/deoxy	100 mM phosphate, 8% PEG 8000	7.0	rt	56
1KD2 <sup>a</sup>	1.87	P2 <sub>1</sub> 2 <sub>1</sub> 2	0.198	T/deoxy	deionized PEG 3350	7.02	rt	64
1RQ3 <sup>a</sup>	1.91	P2 <sub>1</sub> 2 <sub>1</sub> 2	0.167	T/deoxy	10 mM potassium phosphate, 100 mM potassium chloride 10% PEG 6000	7.0	rt	65
1XXT <sup>a</sup>	1.91	P2 <sub>1</sub> 2 <sub>1</sub> 2	0.182	T/deoxy	10 mM potassium phosphate, 100 mM potassium chloride 10% PEG 6000	7.0	rt	55
1BZ0 <sup>a</sup>	1.50	P2 <sub>1</sub>	0.167	T/deoxy	3.6 M ammonium sulfate/phosphate	6.5	rt	66
2D60 <sup>b</sup>	1.70	P2 <sub>1</sub>	0.198	T/deoxy	100 mM (CH <sub>3</sub> ) <sub>2</sub> AsO <sub>2</sub> Na, 75 mM HCl and 16% PEG 6000	5.8	20	59
1HGC	2.10	P2 <sub>1</sub> 2 <sub>1</sub> 2	0.200	T/α-oxy	100 mM phosphate, 8% PEG 8000	7.0	rt	56
1HGB	2.10	P2 <sub>1</sub> 2 <sub>1</sub> 2	0.210	T/aquomet	100 mM phosphate, 8% PEG 8000 and IHP	7.0	rt	56
2DSZ <sup>b</sup>	1.45	P2 <sub>1</sub> 2 <sub>1</sub> 2 <sub>1</sub>	0.187	T/L35, β-aquomet	100 mM (CH <sub>3</sub> ) <sub>2</sub> AsO <sub>2</sub> Na, 75 mM HCl and 16% PEG 6000, 100 μM L35	5.8	20	59
1THB	1.50	P2 <sub>1</sub> 2 <sub>1</sub> 2	0.196	T/IHP, α-oxy	18–25% PEG1000	7.2–7.4		58
1B86	2.5	P2 <sub>1</sub> 2 <sub>1</sub> 2	0.169	T/deoxy, DPG	10 mM sodium phosphate, 18% PEG 1000 and saturated DPG	7.2–7.4	20	57
1YHR <sup>a</sup>	2.6	P2 <sub>1</sub> 2 <sub>1</sub> 2	0.185	T/oxy, IHP	10 mM potassium phosphate, 100 mM potassium chloride, 10% PEG 6000 and 10 mM IHP	7.0	rt	55

<sup>a</sup>PDB coordinates used in our RDC analysis. <sup>b</sup>Data collected at cryogenic condition.

obtained by other methods clearly show that the classical two-structure MWC/Perutz description for hemoglobin allostery as presented in biochemistry, biophysics, and molecular biology textbooks cannot account for Hb function in details and needs revision. In our last review<sup>12</sup> 10 years ago, we gave a summary of our experimental results on the molecular basis of the Bohr effect of Hb A and the solution conformation, dynamics, and subunit communication of Hb A as derived from our nuclear magnetic resonance (NMR) studies. Here, we present new results of NMR and wide-angle X-ray scattering (WAXS) studies that are relevant to the structure–function relationship in hemoglobin.

During the past 10 years, hemoglobin has remained an active research area for biochemical, biophysical, and computational studies with over 6500 papers published in the literature. It is interesting to note that a search of PubMed indicates that there were 489 papers with hemoglobin titles published in 2004, 632 papers in 2009, and 813 papers in 2013. This increase in the number of Hb publications indicates that there are new results as well as new thinking in the field of hemoglobin research. This review is not intended to cover all areas of Hb research but focuses on new findings on the nature of Hb as a dynamic ensemble as related to its properties in solution. For additional readings on Hb and Hb allostery, one could consider a number of relevant articles.<sup>13–31</sup>

## 2. STRUCTURE

From a molecular point of view, Hb A can be considered as a dimer of αβ dimers (Figure 1). The α<sub>1</sub>β<sub>1</sub> and α<sub>2</sub>β<sub>2</sub> dimers come into contact and assume a 2-fold symmetry with the axis passing through a water-filled cavity formed by the four subunits. The B, G, and H helices of the unlike subunits make packing contacts that do not change upon oxygen binding. This “BGH frame” was used to compare the rotational motions of the dimers in going from the T to the R conformation.<sup>32</sup> The C and G helices and FG corner of unlike subunits make “sliding contacts” upon oxygen binding or unloading. Perutz’s structural comparison<sup>3</sup> between the T and the R structures of Hb shows that upon oxygenation (i) the α<sub>2</sub>β<sub>2</sub> dimer rotates approximately 15° relative to the α<sub>1</sub>β<sub>1</sub> dimer, (ii) the heme Fe (II) moves into the porphyrin plane, (iii) six intersubunit salt bridges between α<sub>1</sub> and α<sub>2</sub> (α141Arg–α1Val; α141Arg–α126Asp) and between the α- and β-subunits (α40Lys–β146His) are broken, and (iv) two intra-β-subunit salt bridges (β146His–β94Asp) are broken. These were the observations that formed his stereochemical mechanism to explain Hb allostery. In addition, the T to R structure transition disrupts some interactions (α42Tyr–β99Asp, α97Asn–β99Asp, α91Leu–β40Arg, and α92Arg–β40Arg) and generates new interactions (α38Thr–β97His, α41Thr–β40Arg, and α94Asp–β102Asn) among residues in the α<sub>1</sub>β<sub>2</sub> and α<sub>2</sub>β<sub>1</sub> interfaces.

## 2.1. Crystal Structures of Hemoglobin Determined by X-ray Crystallography

The low-resolution crystal structures of hemoglobin were initially elucidated by Perutz and his colleagues and reported at 5.5 Å resolution almost 60 years ago.<sup>33,34</sup> Since then, more than 200 sets of structural coordinates representing Hb A and its mutants have been deposited with the RCSB (Research Collaboratory Structural Bioinformatics) Protein Data Bank (PDB). The liganded and deoxy forms of Hb A have been reported at 1.25 Å resolution by Park et al.,<sup>35</sup> while Savino et al.<sup>36</sup> solved the structure of the deoxy form of a mutant of Hb A to an even higher resolution (1.07 Å). These newer crystal structures suggest a more complicated picture than the two-structure MWC/Perutz model. Figure 1 shows the crystal structures of Hb A in the deoxy (T type, Figure 1a) and carbonmonoxy (R type, Figure 1b) forms as well as the solution structures of HbCO A (Figure 1c) determined recently by multinuclear NMR spectroscopy. Figure 1d gives a comparison of the average solution structure of HbCO A with R, R2, RR2, and R3 crystal structures.

The methods employed in preparing samples and growing crystals could influence the ultimate structures obtained by X-ray diffraction. Perutz<sup>37</sup> crystallized Hb in high salt and pH 6.5. His protocols had been used by others,<sup>35,38–46</sup> and various representative T and R structures have been obtained and used to compare the structural changes upon ligand binding (Table 1). Alternatively, Hb crystals can be grown in low salt and the presence of polyethylene glycol (PEG). A new form, called R2, was obtained by Silva et al.<sup>47</sup> from crystals grown in low salt (100 mM sodium cacodylate, pH 5.8) and 16% PEG. The  $\alpha_1\beta_1$  dimer is rotated approximately 11° relative to the  $\alpha_2\beta_2$  dimer in the R2 form with respect to R and in a direction different from the T structure.<sup>48,49</sup> The R2 structure is not an artifact due to crystallization at low pH. Similar structures had been reported for a Hb A mutant ( $\beta$ D99Y)<sup>50,51</sup> crystallized in high salt at pH 6.7, and a Hb A, crystallized in low salt and pH 7.4 in the presence of PEG and  $\beta$ -octylglucoside.<sup>52</sup> Using the high-salt condition, Safo and Abraham<sup>53</sup> obtained additional RR2 and R3 quaternary structures at pH 6.7 and 7.1, respectively, for the liganded Hb A. The RR2 model assumes an intermediate conformation between that of the R and R2 structures. The quaternary structural differences between T and R3 are as large as those between T and R2, and the T → R3 and T → R2 transitions are in different directions as defined by a rigid-body screw rotation. Compared to other liganded-Hb structures, the R3 structure has the following features: (i) reduced strain at the  $\alpha$ -heme, (ii) reduced steric contact between the ligands and the distal residues in the  $\beta$ -subunits, (iii) reduced iron–iron distances between  $\alpha_1$ – $\alpha_2$  and  $\beta_1$ – $\beta_2$  subunits, and (iv) both  $\alpha$ - and  $\beta$ -clefts are smaller. Hence, R3 has been postulated to represent the conformation actively involved in ligand uptake and/or release.<sup>54</sup>

In addition to the liganded R structures and unliganded T structures mentioned above, partially liganded T structures have also been reported (Table 1).<sup>55–59</sup> They have been implicated as intermediates in going from the T to the R states of Hb A. Recently, Shibayama et al.<sup>60</sup> obtained a met-Hb crystal in the space group  $C_2$ . The isomorphous crystal contains three tetramers, each representing a distinct conformation between the R and the R2 structures.

The C $\alpha$  atoms from various structures can be superimposed pairwise, and the PyMOL program<sup>61</sup> can then be employed to calculate the root-mean square deviation (RMSD). The

calculated RMSDs for the R–R2 (1.672 Å) and R–R3 (1.923 Å) pairs are significantly larger than that for the R–RR2 (1.120 Å) pair, suggesting that the structure of RR2, not R2 or R3, is closer to that of R. By pairing the R (1IRD) or R2 (1BBB) coordinates with the T (2DN2) structure, we obtained RMSD values of 2.428 and 3.481 Å, respectively, for the R–T and R2–T pairs. Therefore, R is closer to T than is R2, as first reported by Silva et al.<sup>47</sup> Among the nine T-type deoxy structures used in our residual dipolar coupling (RDC) studies (Table 1), the RMSD values between the pairs are quite small (0.130–0.441 Å). However, the 2DN2–1YHR pair<sup>62</sup> has an RMSD of 0.990 Å. 1YHR represents a T-type structure with bound IHP and oxygen. These results clearly show that there are different types of T structure, depending on the experimental conditions.

Dey et al.<sup>63</sup> surveyed the crystallographic quaternary structures of 165 human Hb tetramers. The coordinates were superimposed with the SUPERPOSE program. The relative positioning of the dimer pairs in a tetramer, defined by the polar coordinates of the vector connecting the center of masses of the dimer pairs, was plotted. The liganded-Hbs can be divided into two major clusters, R and Y (R2). Structures that represent the RR2 (1MKO) and R3 (1YZI) forms are clearly outside the clusters. The T cluster representing the deoxy-Hbs can be subdivided according to whether the crystals are monoclinic (space group  $P2_1$ ) formed in high salt or orthorhombic (space groups  $P2_12_12$  or  $P2_12_12_1$ ) formed in low ionic strength and in the presence of PEG. Furthermore, high-oxygen affinity Hb mutants that bind oxygen in the presence of IHP and in the T structure<sup>62</sup> constitute a separate group termed “T<sub>hi</sub>”. This observation is consistent with the RMSD calculations with the PyMOL program.

By varying the experimental conditions, a series of crystal structures has been obtained for Hb in either the T or the R state. With the summaries presented above, there is enough convincing evidence from these crystallographic studies to suggest that Hb can exist in multiple conformations in each state. Thus, X-ray crystallography gives static snapshot views of proteins, which are, in fact, in motion, fluctuating among many conformations.

## 2.2. Solution Structures of Hemoglobin and Effects of Inositol Hexaphosphate Investigated by NMR

The development of high-field, multinuclear, multidimensional NMR, and isotopic labeling techniques have provided powerful tools to investigate the structure and dynamics of proteins in solution. In order to overcome spectral overlap and to facilitate resonance assignments for a protein of the size of hemoglobin (~65 000 Da), we developed a chain-selective labeling technique, in which only one type of Hb chain is isotopically labeled at a time. First, we label the Hb molecule with specific isotopes (<sup>2</sup>H, <sup>13</sup>C, and/or <sup>15</sup>N or all three labels) using our Hb expression plasmid,<sup>67</sup> pHE2. Second, the purified isotopically labeled Hb A is separated into labeled  $\alpha$ - and  $\beta$ -chains. Third, we prepare a chain-selective, isotopically labeled, tetrameric Hb by combining one type of the labeled chain with the other type of unlabeled chain, e.g., combine labeled  $\alpha$ -chains with unlabeled  $\beta$ -chains to produce an  $\alpha$ -chain selectively labeled Hb molecule, and vice versa for a  $\beta$ -chain selectively labeled Hb. The chain-selective labeling of Hb reduces the spectral complexity by 50%, i.e., only the isotopically labeled chain can be observed by heteronuclear NMR. For details, see ref 68. The solution structures of Hb A in both CO and deoxy forms have been investigated by multinuclear NMR methods in two ways,

i.e., (i) exploring the quaternary structures by the NMR residual dipolar coupling (RDC) method<sup>69–73</sup> and (ii) determining the solution structure of Hb A, in particular, the structure of HbCO A, by using stereospecifically assigned methyl groups and RDC values.<sup>74</sup>

**2.2.1. Quaternary Structures of HbCO A and Deoxy-Hb A in Solution.** The method of weak alignment of proteins and the measurement by NMR of the <sup>15</sup>N-<sup>1</sup>H RDCs of the backbone peptide bonds has opened the possibility to investigate the relative orientation of subunits in multisubunit proteins.<sup>75</sup> The measured RDCs can be compared directly with the calculated ones based on the crystal coordinates of the proteins, an excellent way to compare the quaternary structures of Hb in solution and in crystal.

The RDCs of HbCO A aligned with filamentous bacteriophage Pf1 or in a solution of phospholipid bicelles in water as well as in an isotropic medium were measured and compared with the calculated RDCs based on the coordinates of the four R-type crystal structures,<sup>69,70</sup> R (1IRD), R2 (1BBB), RR2 (1MKO), and R3 (1YZI). The top panel of Figure 2

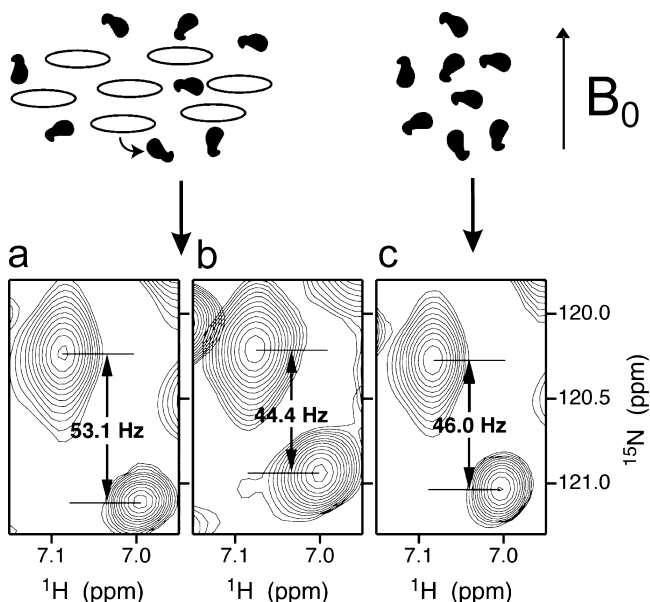


**Figure 2.** (Top) Schematic drawing of proteins and liquid crystals mixture which can generate weak alignment upon application of a magnetic field. Partially aligned molecules (drawing on the left side) yield results in panels a and b, while proteins in isotropic medium (drawing on the right side) yield results in panel c. Reprinted with permission from ref 73. Copyright 2011 Research Signpost. (Bottom) Superimposition of TROSY and HSQC spectra of  $\beta$ -chain specifically (<sup>2</sup>H, <sup>15</sup>N)-labeled HbCO A in 90% H<sub>2</sub>O/10% D<sub>2</sub>O. Cross-peaks of  $\beta$ 65Lys from proteins suspended in (a) lipid bicelle, (b) Pf1 phage, and (c) isotropic media are shown. Reprinted with permission from ref 69. Copyright 2003 National Academy of Sciences.

(taken from Figure 1 of ref 73) gives a schematic representation of proteins suspended in isotropic media or in liquid crystals to generate weak alignment in a magnetic field. The bottom panel of Figure 2 (taken from Figure 1 of ref 69) is a superposition of TROSY and HSQC spectra of HbCO A showing the cross-peaks of  $\beta$ 65Lys in lipid bicelles (a), Pf1 phage (b), and isotropic media (c). The experimentally determined RDCs can be compared with RDCs predicted by calculations based on the X-ray crystal structures for the  $\alpha$ - or  $\beta$ -chains, for an isolated  $\alpha\beta$  dimer, and for the entire tetramer, as presented in Figure 3

(taken from Figure 3 of ref 70). The experimental RDC values for the amino acid residues situated in the rigid  $\alpha$ -helices were compared with those calculated separately for the  $\alpha$ - and  $\beta$ - chains and for the  $\alpha\beta$  dimer using the R and R2 crystal structures. We found that there was no significant difference in the goodness of the fit, as these structures differ mainly in the relative orientation of the  $\alpha_2\beta_2$  and the  $\alpha_1\beta_1$  dimer. It was found, though, that for the entire tetramer, the best match to the experimental data was for a quaternary structure corresponding to a rotation midway between the R and the R2 crystal structures, indicating that the quaternary solution structure of HbCO A was neither that of the classical R structure nor that of the R2 structure.<sup>69</sup>

Because deoxy-Hb is a paramagnetic molecule with four unpaired electrons per heme, partial alignment of this molecule can be achieved solely by the effect of the static magnetic field and RDCs can be obtained by measuring the effective  $J$  coupling ( $J_{\text{HN}} + D_{\text{HN}}$ ) at several magnetic field strengths (Figure 4).<sup>71,72</sup> The calculated RDCs<sup>72</sup> were obtained from eight crystal structures of deoxy-Hb A, 4HHB, 1HGA, 1KD2, 1RQ3, 1XXT, 1BZ0, 2DN2, and 1YHR. The scatter in the eight correlation plots between the observed and the calculated RDCs is larger than the experimental precision. Among the high-resolution deoxy-Hb A structures, 1XXT (with a resolution of 1.91 Å) provides a better fit than the highest resolution structure (2DN2) at 1.25 Å. The measured RDCs were fitted to the  $\alpha_1\beta_1$  dimer and the tetrameric Hb A. Although the best fit is obtained for the dimer, the differences between the dimer and the tetramer fits are small, as shown by the very small difference in the reduced  $\chi^2$  values in Figure 5 (taken from Figure 3 of ref 72). A possible explanation could involve the intradimer dynamics detected by the proton solvent exchange at the  $\alpha_1\beta_1$  (or  $\alpha_2\beta_2$ ) interface. The RDC analysis suggests that the solution structure of deoxy-Hb A differs from all known crystal structures. It is also apparent that IHP affects at least the dimer structure and possibly also the quaternary structure of deoxy-Hb A as evidenced by the much larger reduced  $\chi^2$  values in Figure 5.

The RDC analyses of Hb A in both CO and deoxy forms suggest that the structures of Hb in solution are dynamic ensembles of various structures rather than single static structures.<sup>69–72</sup>

**2.2.2. Solution Structure of HbCO A and Effects of IHP.** The solution structure of HbCO A determined by NMR has been further refined by using backbone NH RDCs and stereospecifically assigned methyl groups.<sup>69,70,74,76</sup> The NMR experiments were carried out in 0.1 M sodium phosphate at pH 7.0 and 30 °C. The details of the 20 lowest energy structures of HbCO A in solution were deposited in the PDB (entry 2M6Z).<sup>74</sup> For structural statistics for the 20 HbCO A conformers, see Table 1 of ref 74. Figure 1c gives the 10 lowest energy solution structures of HbCO A.<sup>74</sup> Both  $\alpha$ - and  $\beta$ - chains assume tertiary structures similar to the X-ray crystal structures. However, the tetrameric quaternary structure determined by NMR exhibits a closer resemblance to the R than to the R2 structure determined by X-ray crystallography as shown in Figure 6c and 6d (taken from Figure 1 of ref 74). For the switch region of the  $\alpha_1\beta_2$  interface, the NMR structures of HbCO A resemble the R and R2 structures and differ significantly from the T structure with respect to the location of  $\beta_2$ 97His (Figure 6e). The complete 3D solution structure of deoxy-Hb A is yet to be determined.

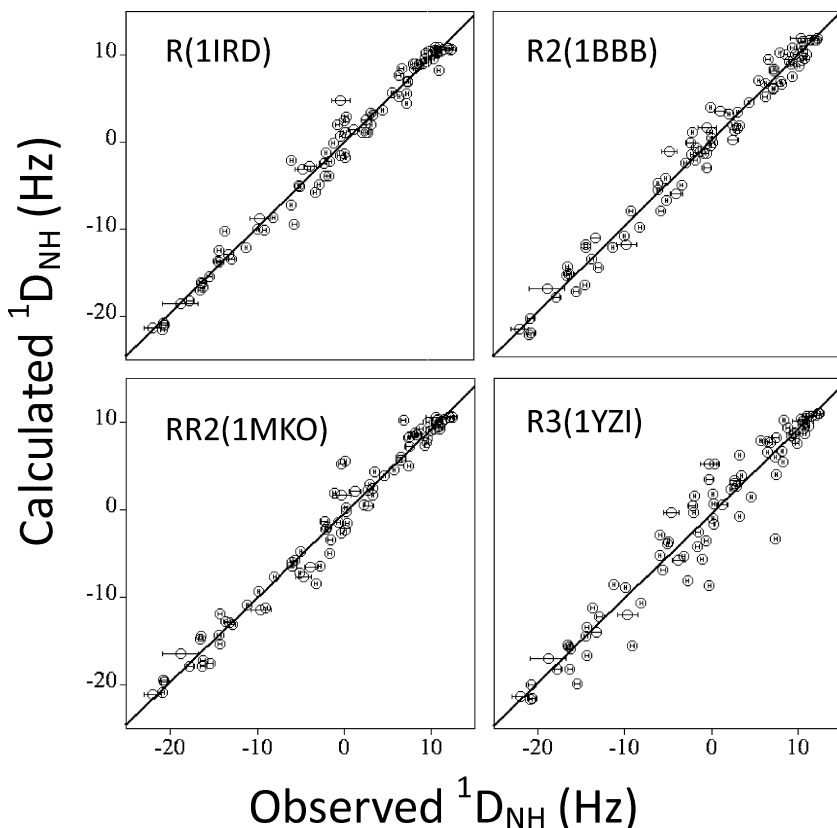


**Figure 3.** Observed RDCs plotted against those calculated according to the coordinates of crystal structures R (1IRD), R2 (1BBB), RR2 (1MKO), and R3 (1YZI). The quality factors ( $Q$ ) of the plots are 14.6%, 15.2%, 17.9%, and 26.4%, respectively.<sup>179</sup> The error in each RDC measurement, shown as a horizontal error bar, was calculated from the line width and signal-to-noise ratio of the corresponding cross-peaks.<sup>180</sup> Reprinted with permission from ref 70. Copyright 2006 American Chemical Society.

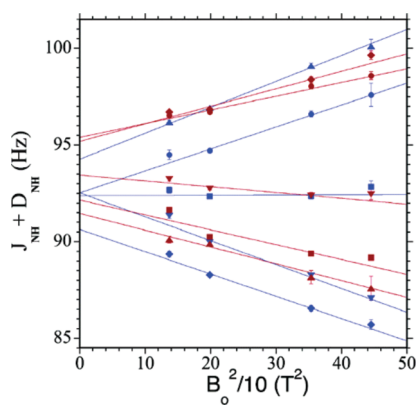


**Figure 4.** Magnetic field dependence of observed ( ${}^1J_{\text{NH}} + {}^1D_{\text{NH}}$ ) couplings of chain-specific ( ${}^{15}\text{N}$ ,  ${}^2\text{H}$ )-labeled recombinant deoxy-Hb A. As a demonstration, five amino acid residues each are selected from the  $\alpha$ - and  $\beta$ -chains of Hb A:  $\alpha$ 39Thr (blue ●) and  $\beta$ 24Gly (red ●),  $\alpha$ 45His (blue ♦) and  $\beta$ 25Gly (red ♦),  $\alpha$ 46Phe (blue ▽) and  $\beta$ 30Arg (red ▽),  $\alpha$ 81Ser (blue ■) and  $\beta$ 39Gln (red ■), and  $\alpha$ 96Val (blue ▲) and  $\beta$ 42Phe (red ▲). ( ${}^1J_{\text{NH}} + {}^1D_{\text{NH}}$ ) values in Hertz are plotted versus the square of the magnetic field ( $B_0$ ) in  $\text{T}^2$  ( $\text{Tesla}^2$ ). Data points are fitted to the equation  ${}^1J_{\text{NH}} = {}^1J_{\text{NH}}(\text{iso}) + cB_0^2$ , where  $c$  is the slope. Y intercept of each plot gives  ${}^1J_{\text{NH}}(\text{iso})$ , which represents the true isotropic  ${}^1J_{\text{NH}}$  value and is used for determination of RDCs. Reprinted with permission from ref 72. Copyright 2006 American Chemical Society.

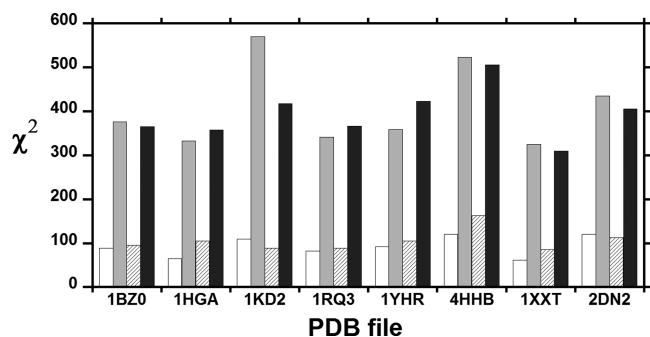


**Figure 5.** Fitting quality of experimentally determined RDCs versus those calculated from X-ray crystal structures of deoxy-Hb A. PDB code of each X-ray crystal structure is shown along the  $x$  axis, and the corresponding reduced  $\chi^2$  values of the fit to either the  $\alpha_1\beta_1$  dimer (blank in the absence and gray in the presence of IHP) or the whole tetramer (striped in the absence and black in the presence of IHP) are along the  $y$  axis. Adapted with permission from ref 72. Copyright 2007 American Chemical Society.

BPG and IHP to deoxy-Hb A were investigated by X-ray crystallography and model building experiments.<sup>77,78</sup> However, the exact binding sites for these two allosteric effectors in the Hb molecule remain controversial. Recently, we investigated by heteronuclear NMR the binding of IHP and its effects on the structure of HbCO A. Using the chemical shift perturbations caused by the presence of IHP, four putative IHP binding regions were identified in HbCO A, namely, (i) around the N-termini ( $\alpha$ 1Val,  $\alpha$ 3Ser,  $\alpha$ 7Lys,  $\alpha$ 9Asn,  $\beta$ 1Val, and  $\beta$ 3Leu) and

426 The allosteric effectors, 2,3-BPG and IHP, significantly affect  
427 the oxygen binding affinity of Hb A. The binding sites for 2,3-

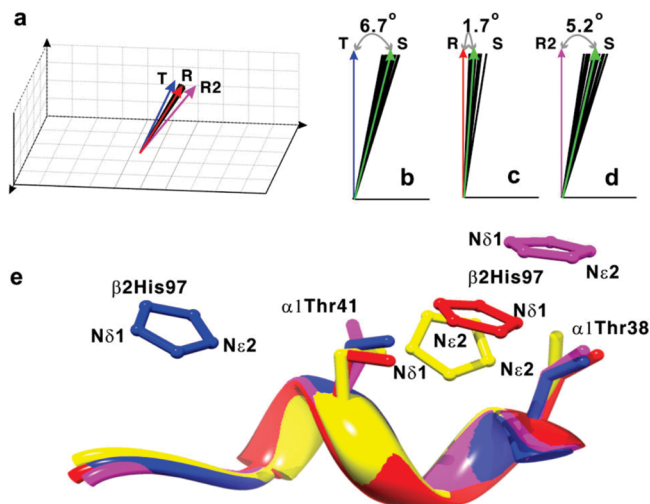


**Figure 6.** Comparison of the symmetric axis orientations (a–d) and the switch region in the  $\alpha_1\beta_2$  interface (e) of the 20 lowest energy solution conformations of HbCO A with those of the T, R, and R2 crystal structures. (a) Distribution of the C<sub>2</sub> axes of different structures in a three-dimensional frame. (b, c, and d) Angles between the average of the 20 lowest energy NMR structures (represented with green arrows) and the C<sub>2</sub> axes of the T, R, and R2 structures, respectively. Angles shown in panels b–d are drawn off scale and enlarged for better visualization. (a) C<sub>2</sub> axes of the T, R, R2, and 20 solution conformations are shown as blue, red, magenta, and black lines, respectively. (e) Switch regions in the T, R, R2, and one representative solution conformation are colored blue, red, magenta, and yellow, respectively. Backbone atoms of residues 38–44 in the  $\alpha_1$  subunit are superimposed to illustrate the relative orientation of  $\beta_2$ His97. Reprinted with permission from ref 74. Copyright 2013 American Chemical Society.

the C-termini ( $\alpha$ 137Thr,  $\beta$ 143His, and  $\beta$ 146His), (ii) around the EF loop ( $\alpha$ 78Asn,  $\alpha$ 79Ala,  $\beta$ 82Lys, and  $\beta$ 83Gly), (iii) around the switch region of the  $\alpha_1\beta_2$  interface composed of the  $\alpha$ C helix and the  $\beta$ FG corner ( $\alpha$ 38Thr,  $\alpha$ 39Thr,  $\alpha$ 41Thr,  $\beta$ 96Leu,  $\beta$ 99Asp, and  $\beta$ 101Glu) and around the joint region makes up of the  $\alpha$ FG corner and the  $\beta$ C helix ( $\alpha$ 94Asp,  $\alpha$ 96Val,  $\alpha$ 97Asn,  $\alpha$ 100Leu, and  $\beta$ 41Phe), and (iv) around the heme group ( $\alpha$ 65Ala,  $\alpha$ 83Leu,  $\alpha$ 86Leu,  $\alpha$ 136Leu,  $\beta$ 67Val,  $\beta$ 70Ala,  $\beta$ 88Leu,  $\beta$ 98Val, and  $\beta$ 141Leu). According to the docking calculations using the solution structure of HbCO A, the central cavity has a single binding site for IHP, while the  $\beta$ -cleft located

at the entrance of the central cavity and the  $\alpha$ -cleft have two potential binding sites each. For details, see Figure 7 (taken from Figure 4 of ref 74). The chemical shifts for a number of amino acid residues that are not located on the protein surface have also been perturbed. This suggests that IHP binding not only affects local structures but also disturbs regions away from the binding site. Therefore, it is difficult to determine the exact locations of the binding sites using only the chemical-shift-perturbation data. The perturbation of chemical shifts was found to depend on the IHP concentration, and the binding affinity was estimated to be submillimolar, but it could not be quantified without knowing the exact number of IHP binding sites. Zuiderweg et al.<sup>79</sup> used <sup>31</sup>P NMR to approximate the affinity of IHP to HbCO at  $\sim$ 50  $\mu$ M, compatible with our result.

We found that IHP binding induces significant changes in the chemical shifts of nearly all of the methyl groups around the heme moiety and the methyl side chains located around it cannot be in direct contact with the bound IHP. Therefore, IHP binding induces tertiary structural changes around the heme and thus causes the observed chemical-shift perturbation for the methyl groups around it. The results support the global allostery model, which stipulates that heterotropic effectors change the tertiary structure of Hb and could alter the oxygen-binding affinity.<sup>8,80</sup> IHP binding also changes the chemical shifts of many methyl-containing residues located in the  $\alpha_1\beta_2$  interface and several residues in the  $\alpha_1\beta_1$  interface. Again, these residues could not be in direct contact with IHP. Thus, these changes in chemical shifts reflect a change in the quaternary structure of HbCO A upon IHP binding. These findings are in agreement with our RDC and backbone relaxation studies.<sup>70,81</sup> Hence, upon IHP binding, HbCO A changes its quaternary structure and also the tertiary structures around the heme groups. Both structural changes can affect the affinity of Hb for its ligands, e.g., O<sub>2</sub>, CO, or NO.

### 2.3. Wide-Angle X-ray Scattering Investigation of Hemoglobin Structures in Solution

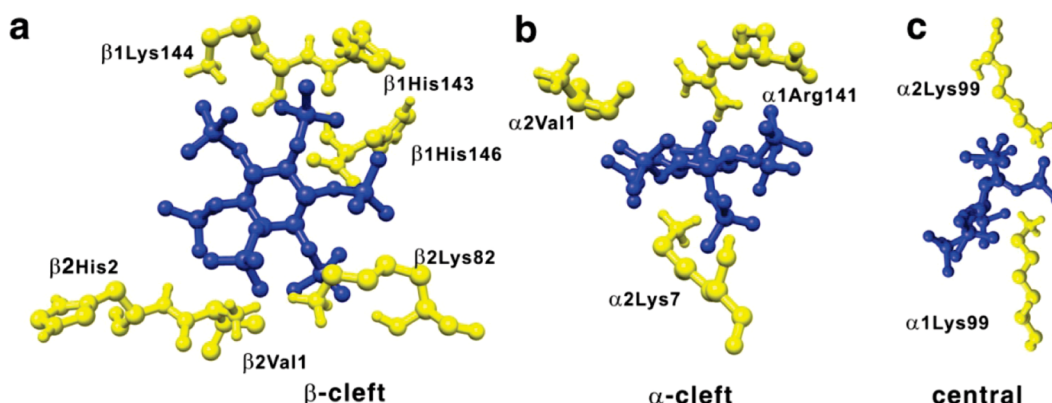


**Figure 7.** Putative IHP binding sites in the  $\beta$ -cleft (a),  $\alpha$ -cleft (b), and central cavity (c) of Hb A. IHP molecule is presented as blue sticks. Reprinted with permission from ref 74. Copyright 2013 American Chemical Society.

parameters.<sup>82</sup> WAXS can distinguish between similar structures and provide information on the structural fluctuations of proteins in solution.<sup>83,84</sup> This technique was applied to investigate the structural and dynamic properties of Hb in the CO, deoxy, and met forms.<sup>84</sup> The Hb samples were prepared in 0.05 M sodium phosphate at pH 7.0 with the Hb concentrations at 50, 20, and 10 mg/mL. WAXS experiments were carried out in a flow cell at 4 °C. Met-Hb A and HbCO A have similar WAXS patterns that are different from that of deoxy-Hb A. The results confirm the well-known relationships among these structures as defined by X-ray crystallography. The discrepancy between the calculated and the observed patterns for myoglobin (Mb) (Figure 3c of ref 84) is likely due to small fluctuations in Mb structure in solution as explained previously.<sup>85</sup> The much larger discrepancy between the calculated results based on the atomic coordinates for HbCO A (2DN3) and the observed data for Hb cannot be explained by structural fluctuations alone, indicating that the quaternary structure of HbCO A in solution is dissimilar from that in the crystal.<sup>84</sup> This finding could be explained by a dynamic ensemble of structures of HbCO A in solution consistent with the NMR results described above.

The WAXS pattern from rHbCO ( $\alpha$ V96W/ $\beta$ N108 K), a low-affinity mutant with substitutions at the  $\alpha_1\beta_2$  ( $\alpha$ V96W) and  $\alpha_1\beta_1$  ( $\beta$ N108 K) interfaces, appears to be an intermediate between HbCO A and deoxy-Hb A. These effects appear to be mediated by quaternary structural changes, since NMR studies indicate that this mutant rHb exhibits properties intermediate between the R and the T states, and the protein is capable of switching its quaternary structure from the R state to the T state even when liganded.<sup>86</sup> Another interesting observation is that the WAXS patterns indicate that deoxy-Hb A exhibits substantially larger structural fluctuations than HbCO A, consistent with a recent molecular dynamics study that suggests increased dynamics is associated with lowered oxygen affinity.<sup>21</sup> A similar difference in the dynamics between liganded and unliganded HbA was also observed in the intradimeric  $\alpha_1\beta_1$  and  $\alpha_2\beta_2$  interfaces,<sup>87</sup> showing increased mobility correlated with decreased affinity as reported by water proton exchange of the NH side chains of  $\alpha$ 103His.

Given the extensive crystallographic studies of Hb, the close similarity of all crystal T-state quaternary structures would seem to imply a narrow structural ensemble in solution, whereas the multiple distinct quaternary structures observed for liganded-Hbs might imply sampling of a far broader structural ensemble. However, the relationship between polymorphism in solution and polymorphism of crystallographic structures is not well understood. It could equally well be the case that the energy landscape for unliganded-Hb is smooth and broad, resulting in a single "selected" quaternary structure for many different crystallographic conditions, whereas the energy landscape for liganded-Hb might be rough and relatively narrow, making possible selection of multiple distinct quaternary structures during diverse crystallographic experiments. One might speculate that a broad, smooth energy landscape could provide a kinetic advantage for oxygen binding, whereas an irregular landscape may provide for conformations consistent with different levels of partial ligation.

### 3. DYNAMICS

Multinuclear NMR spectroscopy is also an excellent tool to investigate the dynamic properties of the polypeptide backbone and side-chain residues of Hb A on the time scales of

picosecond to nanosecond and microsecond to millisecond. Having completed the assignments of the polypeptide backbones<sup>88,89</sup> of deoxy- and CO-forms of Hb A, the indole NH of the Trp residues,<sup>68</sup> and the methyl groups<sup>74</sup> of HbCO A, we investigated the dynamic properties of the backbones, Trp side chains, and methyl groups by NMR in the absence and presence of IHP. In addition, the amide–water proton exchange experiments can provide valuable information in the subsecond time scale for amino acid residues located in the subunit interfaces and the loop regions.

#### 3.1. Backbone Dynamics Analyzed by $^{15}\text{N}$ Relaxation Parameters

The amide N–H bonds of most amino acid residues are rigid in both deoxy and CO forms of Hb A on the fast time scale (picoseconds to nanoseconds)<sup>81,90</sup> as shown by Model-free-based NMR dynamics analysis.<sup>91</sup> However, there is considerable flexibility in the loop regions, certain helix–helix connections, the intradimer interface (i.e., B, G, and H helices and the GH corner) and for several amino acid residues (e.g.,  $\alpha$ 31Arg,  $\beta$ 3Leu,  $\beta$ 41Phe,  $\beta$ 123Thr, and  $\beta$ 146His) that are possibly involved in the allosteric pathway. The residues  $\alpha$ 31Arg and  $\beta$ 123Thr, neighbors in the intradimer ( $\alpha_1\beta_1$ ) interface, appear flexible in deoxy-Hb A and become more rigid upon CO binding. This may imply a role for  $\alpha$ 31Arg and  $\beta$ 123Thr in intradimer ( $\alpha_1\beta_1$ ) communication, not predicted from the crystal structure.

Several amino-acid residues in Hb A appear to show slow conformational mobility (microseconds to milliseconds time scale), which has been characterized by  $R_{\text{ex}}$  mapping experiments.<sup>92</sup> Conformational exchanges occur in several amino acid residues,<sup>90</sup> such as  $\beta$ 109Val and  $\beta$ 132Lys in deoxy-Hb A and  $\alpha$ 40Lys in HbCO A.

The mobility of  $\beta$ 109Val at the intradimer interface ( $\alpha_1\beta_1$  or  $\alpha_2\beta_2$ ) of deoxy-Hb A is not consistent with the crystallographic observations that show rigid packing at this site.<sup>1,32,42</sup> On the other hand, the mobility of  $\alpha$ 40Lys in HbCO A shown in the  $R_{\text{ex}}$  mapping experiments is consistent with the observation from the crystallographic data, which show that the H bond between  $\alpha$ 40Lys and  $\beta$ 146His in deoxy-Hb A is absent in HbCO A, as a result of breaking a strong interaction in the interdimer interfaces ( $\alpha_1\beta_2$  or  $\alpha_2\beta_1$ ) due to the allosteric transition.<sup>32</sup>

Backbone dynamics studies<sup>90</sup> indicate that the binding of IHP has distinct effects on the dynamics of the T and R states of Hb A. In the absence of IHP, the majority of the polypeptide backbone amino acid residues of HbCO A and deoxy-Hb A are not mobile on the microsecond to millisecond time scale with the exception of several amino acid residues,  $\beta$ 109Val and  $\beta$ 132Lys in deoxy-Hb A and  $\alpha$ 40Lys in HbCO A. IHP binding appears to rigidify  $\alpha$ 40Lys in HbCO A but does not significantly affect the flexibility of  $\beta$ 109Val in deoxy-Hb A. Conversely, in the presence of IHP, several amino acid residues, especially those at the interdimer ( $\alpha_1\beta_2$  or  $\alpha_2\beta_1$ ) interface of HbCO A, exhibit conformational exchange, such as the proximal  $\beta$ 92His in the  $\beta$ -subunit heme pocket as well as other residues located in the flexible joint ( $\beta$ C helix– $\alpha$ FG corner) and the switch region ( $\alpha$ C helix– $\beta$ FG corner) that play an important role in the dimer–dimer rotation of Hb during the oxygenation process. It appears that the IHP-induced quaternary structural fluctuation could be a factor in reducing the ligand affinity of liganded Hb. See also the results discussed in the section on methyl dynamics.

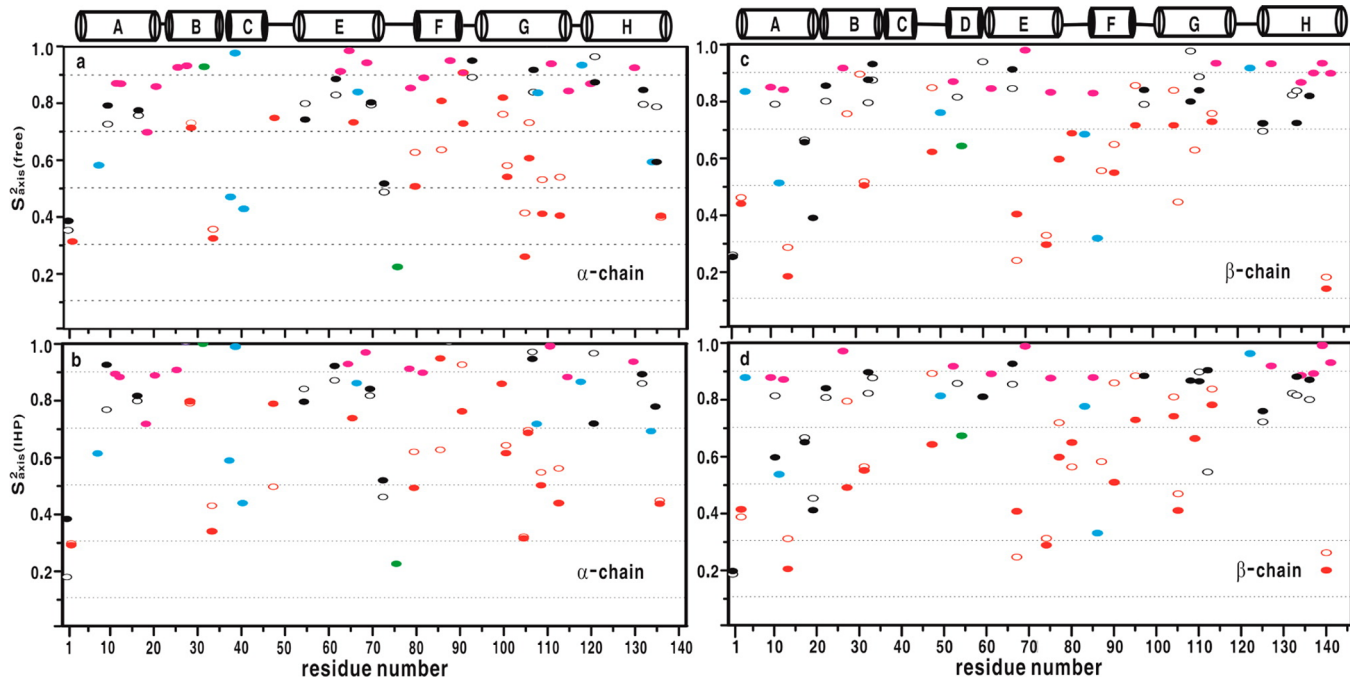


**Figure 8.** Order parameters ( $S_{\text{axis}}^2$ ) describing the degree of spatial restriction of the  $C_3$ -symmetric axis for methyl groups in the  $\alpha$ - and  $\beta$ -chains in the absence (a and c, respectively) and presence (b and d, respectively) of IHP. Uncertainties in  $S_{\text{axis}}^2$  for most methyl groups were  $\sim 0.01$ , and maximal uncertainty was  $\sim 0.02$ . Ala, Leu, Met, Thr, and Val methyls are colored magenta, red, green, light blue, and black, respectively. *pro-R* and *pro-S* methyl groups for Val and Leu are represented with empty and filled circles, respectively. Reprinted with permission from ref 74. Copyright 2013 American Chemical Society.

### 3.2. Dynamics of Tryptophan Residues Analyzed by $^{15}\text{N}$ Relaxation Parameters

There are six Trp residues in the Hb A molecule, three for each  $\alpha\beta$  dimer.  $\alpha 14\text{Trp}$  and  $\beta 15\text{Trp}$  are located in interhelical positions within their respective subunits, while the two  $\beta 37\text{Trp}$  residues are situated in the intersubunit ( $\alpha_1\beta_2$  and  $\alpha_2\beta_1$ ) interface.<sup>1</sup> Due to the symmetry of the molecule, there is only one signal for each subunit type, so that three peaks are observed for the indole NH in the HSQC spectra, one for each Trp type, well resolved from the amide peaks and their chemical shifts change when hemoglobin binds oxygen or CO, the largest change being for  $\beta 37\text{Trp}$ . The side chain of  $\beta 37\text{Trp}$  was found to be involved in a relatively slow conformational exchange on the microsecond to millisecond time scale as detected by a Model-free analysis and the transverse relaxation dispersion method<sup>93,94</sup> under certain experimental conditions.<sup>95</sup>

The side chain of  $\beta 37\text{Trp}$  is a sensitive reporter for the structural and dynamic changes that occur in the  $\alpha_1\beta_2$  and  $\alpha_2\beta_1$  subunit interfaces due to the T to R transition. Amino acid substitutions in the  $\alpha_1\beta_2$  (or  $\alpha_2\beta_1$ ) subunit interface and the presence of IHP affect the dynamics of  $\beta 37\text{Trp}$ . For example,  $\beta 37\text{Trp}$  in HbCO A exhibits conformational exchange only in the presence of IHP, implying a conformational exchange on the millisecond time scale as evidenced by the relaxation dispersion experiments, while the conformational exchange of  $\beta 37\text{Trp}$  is observed in a low-affinity mutant, rHb ( $\alpha V96W$ ), in the CO form even in the absence of IHP and also in a high-affinity mutant, rHb Kempesy ( $\beta D99N$ ), in the deoxy form.<sup>95</sup>

The other two tryptophan residues,  $\alpha 14\text{Trp}$  and  $\beta 15\text{Trp}$ , form H bonds with  $\alpha 67\text{Thr}$  and  $\beta 72\text{Ser}$ , respectively, to connect the A and E helices in the  $\alpha$ - and  $\beta$ -subunits. No conformational exchange on the microsecond to millisecond time scale is observed for these residues.<sup>95</sup> It should be noted

that the dynamical roles of the side chains of  $\alpha 14\text{Trp}$  and  $\beta 15\text{Trp}$  were also explored by time-resolved UV resonance Raman spectroscopy<sup>96,97</sup> with recombinant site-specific mutants of Hb A. It was found that the absence of these interhelical H bonds in the mutants has negligible effects on the oxygen affinity and cooperativity of Hb. However, a full complement of the H bonds can slow down the initial quaternary motion in Hb but accelerate the interdimer motions that produce the T-state contacts. These findings provide a new insight into the roles of H bonds at the intradimer  $\alpha_1\beta_1$  (or  $\alpha_2\beta_2$ ) interface.

### 3.3. Dynamics of Methyl Groups Analyzed by $^{13}\text{C}$ Relaxation Parameters

The  $S_{\text{axis}}^2$  values of the methyl groups reflect the degree of spatial restriction of the  $C_3$  symmetric axis. The average  $S_{\text{axis}}^2$  values of HbCO A were found to be 0.70 for the  $\alpha$ -chain and 0.65 for the  $\beta$ -chain,<sup>74</sup> which are lower than the  $S^2$  values for the backbone dynamics.  $S_{\text{axis}}^2$  values of the methyl groups vary in a similar range as  $S^2$  values,<sup>81,90</sup> especially when the methyl group is very close to the backbone, such as that in Ala residue.

The dynamics of the methyl groups is not always the same as that of the backbone. The former is also dependent on how far the methyl group is from the backbone.<sup>98</sup> The  $S_{\text{axis}}^2$  values of residues Thr, Val, and Leu are less related to the secondary structure. Some residues in the  $\alpha$ -helical elements have small (more flexible)  $S_{\text{axis}}^2$  values, while others located in the loop regions show relatively large  $S_{\text{axis}}^2$  (less flexible) values,<sup>74</sup> suggesting that the  $S_{\text{axis}}^2$  values of these methyl groups are more likely affected by other factors.

One of the factors that could affect the  $S_{\text{axis}}^2$  values is whether the methyl groups are buried or exposed to solvent. On the basis of the R, R2, and NMR structures, the methyl groups of  $\alpha 39\text{Thr}$  and  $\alpha 108\text{Thr}$  are completely buried inside the protein

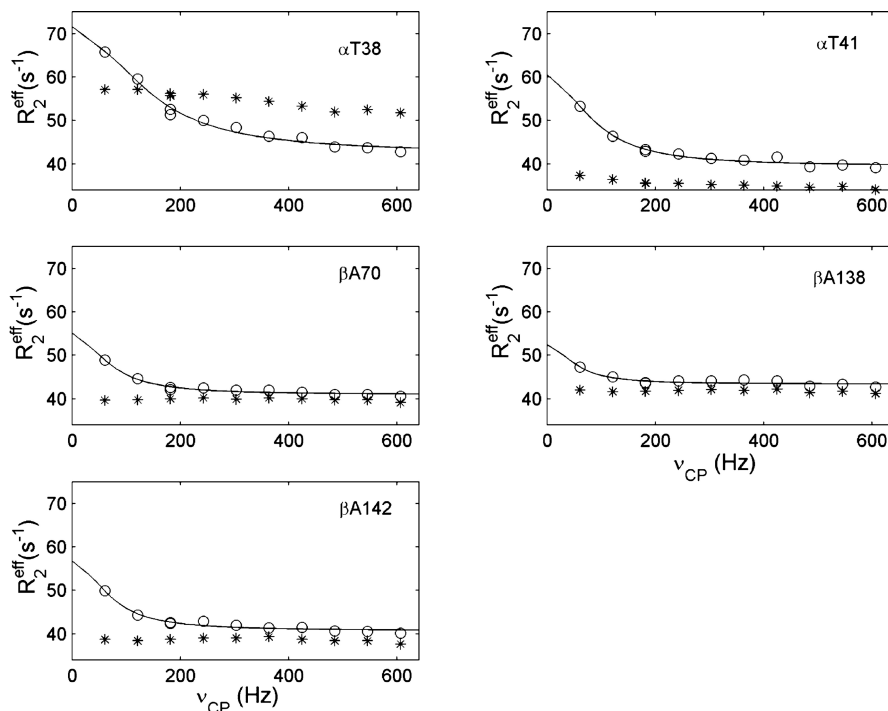


**Figure 9.** Relaxation dispersion profiles of the methyl groups with intrinsic conformational exchange in the absence (asterisks) and presence (circles) of IHP. Solid lines are fitted to the data points according to a two-state exchange model. Each panel represents the amino acid as indicated. Reprinted with permission from ref 74. Copyright 2013 American Chemical Society.

molecule; their  $S_{\text{axis}}^2$  values are 0.95 and 0.81, respectively, and are significantly larger than the average. For partially solvent-exposed methyl groups, the  $S_{\text{axis}}^2$  values were found to be either lower than the average (e.g., 0.58 for  $\alpha$ 8Thr, 0.51 for  $\beta$ 12Thr, and 0.31 for  $\beta$ 87Thr) or significantly higher than the average (0.81 for  $\alpha$ 67Thr, 0.91 for  $\alpha$ 118Thr, 0.81 for  $\beta$ 4Thr, 0.73 for  $\beta$ 50Thr, and 0.89 for  $\beta$ 123Thr).

The  $S_{\text{axis}}^2$  values also relate to the dynamics in the interfaces of Hb A. For example, the  $S_{\text{axis}}^2$  values of  $\alpha$ 38Thr and  $\alpha$ 41Thr are 0.47 and 0.43, respectively, significantly smaller than the average value (0.70), suggesting that the side-chain methyl groups in the  $\alpha_1\beta_2$  interface are more dynamic than those in the  $\alpha_1\beta_1$  interface. The larger  $S_{\text{axis}}^2$  values of some methyl groups are usually consistent with the existence of H bonds observed in the X-ray crystal structures, which could be used to identify the local H bonds. The side-chain oxygen atoms of  $\alpha$ 118Thr,  $\beta$ 4Thr,  $\beta$ 50Thr, and  $\beta$ 123Thr can form H bonds with their proximal backbone NH hydrogen atoms of  $\alpha$ 121Val,  $\beta$ 7Glu,  $\beta$ 53Ala, and  $\beta$ 126Val, respectively. A H bond between the side-chain OH of  $\alpha$ 118Thr to the backbone NH of  $\alpha$ 121Val can be formed because this distance is 3.02 Å, according to the R2 crystal structure (1BBB), for example. Similarly, the corresponding distances for  $\beta$ 4Thr,  $\beta$ 50Thr and  $\beta$ 123Thr's  $\gamma$ -OH to the backbone NH of  $\beta$ 7Glu,  $\beta$ 53Ala, and  $\beta$ 126Val are 2.98, 2.94, and 2.98 Å, respectively.

In the X-ray crystal structures of HbCO A, the H bond between the OH group of  $\alpha$ 41Thr and the side-chain NH<sub>2</sub> hydrogen atom of  $\beta$ 40Arg is predicted in the R structure, not in the R2 structure. If the side-chain hydroxyl group of Thr is involved in H bonding, the motion of the C<sub>β</sub>-C<sub>γ</sub> bond would be greatly restricted and the  $S_{\text{axis}}^2$  value should be quite large. In fact, the  $S_{\text{axis}}^2$  value of  $\alpha$ 41Thr is small (0.43), suggesting that the side chain of this residue is flexible. Thus, the local solution conformation at these two residues could be closer to the R2

than the R structure, although the overall solution structure is more similar to the R than the R2 structure in terms of the relative orientation of the two  $\alpha\beta$  dimers. Another example is the H bond between the side chain of  $\alpha$ 67Thr and the side-chain NeHe of  $\alpha$ 14Trp. The H bond can only exist in the R2 structure, not in the R structure.

The dynamics of the side-chain methyl groups in the picosecond to nanosecond and microsecond to millisecond time scales can be used to identify the binding sites of IHP in HbCO A and also demonstrate the allosteric effects of IHP, as summarized in Figures 8 and 9 (taken from Figure 5 and 6 of ref 74). The addition of IHP to HbCO A affects the mobility of several methyl groups; some become more flexible while others become more rigid. The amino acid residues with significant changes in  $S_{\text{axis}}^2$  values are distributed mainly in the putative IHP binding sites mentioned earlier.

Slower motions detected by the conformational exchange were only observed for the methyl groups of  $\alpha$ 38Thr and  $\alpha$ 41Thr, indicating that the switch region in the  $\alpha_1\beta_2$  interface of HbCO A is dynamic on the microsecond to millisecond time scale. Meanwhile, the methyl groups of Ala, Met, and other Thr residues in HbCO A do not display relaxation dispersion in the absence of IHP (Figure 9, taken from Figure 6 of ref 74). The conformational exchange described here is consistent with the results from our backbone relaxation study, i.e., the IHP-induced conformational exchange has been detected in three regions, namely, the  $\alpha_1\beta_2$  interface, heme pockets, and the presently putative IHP-binding sites.<sup>90</sup> Localized conformational exchange in the  $\alpha_1\beta_2$  interface was also detected early on for the indole NH group of  $\beta$ 37Trp in HbCO A in the presence of IHP.<sup>95</sup>

The dynamics of the backbone and the side-chain methyl groups show that IHP binds to many sites in HbCO A, which is consistent with early <sup>31</sup>P NMR studies<sup>99</sup> on binding of IHP to

745 HbCO A with exchange rates greater than  $10^4$  s<sup>-1</sup>. The  
 746 conformational exchange observed in our experiments could  
 747 arise from the relative movement of the  $\alpha_1\beta_1$  dimer with respect  
 748 to the  $\alpha_2\beta_2$  dimer. These motions could alter the local  
 749 structures as manifested in changes in the chemical shifts  
 750 around the  $\alpha_1\beta_2$  interface and also around the heme pockets,  
 751 thus modulating the oxygen affinity of the Hb molecule.

### 3.4. Amide–Water Exchange Measured by NMR

752 Amide–water exchange experiments provide a way to measure  
 753 the dynamics of amino acid residues on the subsecond time  
 754 scale. Experiments were carried out on chain-specifically <sup>2</sup>H-  
 755 and <sup>15</sup>N-labeled HbCO A samples by using the phase-  
 756 modulated CLEAN chemical exchange with a fast HSQC  
 757 detection scheme.<sup>100</sup> Table 2 (taken from Table 3 of ref 74)

**Table 2. Water–Amide Proton Exchange Rates for HbCO A in the Absence and Presence of IHP<sup>a</sup>**

residue	$k_{ex}$ (s <sup>-1</sup> ) without IHP	$k_{ex}$ (s <sup>-1</sup> ) with IHP	intrinsic $k_{ex}$ (s <sup>-1</sup> ) <sup>c</sup>
$\alpha$ 5Ala	15.7 ± 0.1	34.2 ± 1.0	15.0
$\alpha$ 20His	2.6 ± 0.2	2.5 ± 0.1	43.7
$\alpha$ 22Gly	34.7 ± 0.2	35.3 ± 0.6	48.6
$\alpha$ 38Thr	38.3 ± 0.7	19.3 ± 0.8	12.8
$\alpha$ 45His	5.4 ± 0.1	4.6 ± 0.4	25.1
$\alpha$ 50His	60.3 ± 0.3	52.0 ± 0.8	87.2
$\alpha$ 51Gly	43.7 ± 0.4	39.9 ± 0.6	119.0
$\alpha$ 52Ser	2.3 ± 0.1	2.4 ± 0.1	90.5
$\alpha$ 53Ala	63.1 ± 0.9	66.1 ± 0.5	52.1
$\alpha$ 54Gln	6.1 ± 0.1	6.8 ± 0.2	30.0
$\alpha$ 74Asp	3.7 ± 0.1	3.7 ± 0.1	9.5
$\alpha$ 82Ala	35.6 ± 0.1	19.5 ± 0.2	52.1
$\alpha$ 115Ala	11.1 ± 0.2	11.5 ± 0.3	15.0
$\beta$ 3Leu	4.3 ± 0.3	1.5 ± 0.1	16.8
$\beta$ 6Glu	3.7 ± 0.1	5.5 ± 0.4	4.7
$\beta$ 19Asn	4.8 ± 0.2	5.6 ± 0.1	58.4
$\beta$ 41Phe	b	40.4 ± 2.0	24.9
$\beta$ 44Ser	28.8 ± 0.5	48.7 ± 0.7	43.5
$\beta$ 47Asp	4.2 ± 0.1	7.5 ± 0.2	17.3
$\beta$ 52Asp	1.3 ± 0.1	4.0 ± 0.2	7.6
$\beta$ 78Leu	b	1.2 ± 0.1	16.8
$\beta$ 79Asp	6.4 ± 0.2	5.7 ± 0.1	10.2
$\beta$ 81Leu	59.6 ± 0.8	19.4 ± 0.8	14.3
$\beta$ 82Lys	14.8 ± 0.3	b	14.7
$\beta$ 87Thr	16.9 ± 0.4	17.1 ± 0.3	22.2
$\beta$ 120Lys	5.2 ± 0.2	7.2 ± 0.4	35.2

<sup>a</sup>Measurements were carried out in 0.1 M sodium phosphate at pH 7.0 and 30 °C using a Bruker 800-MHz spectrometer. Reprinted with permission from ref 74. Copyright 2013 American Chemical Society.

<sup>b</sup>Exchange rates of <1 s<sup>-1</sup>, which are undetectable. <sup>c</sup>Intrinsic exchange rates derived using SPHERE (<http://www.fccc.edu/research/labs/roder/sphere/>).

(Table 2). Thus, this region of the  $\alpha_1\beta_2$  interface is dynamic on 769 the millisecond to second time scale and is accessible to water. 770

The binding of IHP to HbCO A does not change 771 significantly the exchange rates for most amides (Table 2). 772 The result implies that IHP binding does not cause significant 773 secondary structural and dynamic changes in the Hb molecule. 774 The few noticeable exceptions are  $\alpha$ 5Ala,  $\beta$ 41Phe, and  $\beta$ 44Ser. 775 The exchange rates for these residues increase by more than 10 776 s<sup>-1</sup>. Conversely, the exchange rates for  $\alpha$ 38Thr,  $\alpha$ 82Ala, 777  $\beta$ 81Leu, and  $\beta$ 82Lys decrease by more than 10 s<sup>-1</sup>. The 778 reduced exchange rates for  $\beta$ 81Leu and  $\beta$ 82Lys can be 779 explained by their locations at one of the putative IHP-binding 780 sites, and the bound IHP can block water from accessing to the 781 amides of these two residues.  $\alpha$ 38Thr,  $\beta$ 41Phe, and  $\beta$ 44Ser 782 residues are located in the switch or joint region of the  $\alpha_1\beta_2$  783 interface. These residues experience significant changes in the 784 exchange rates. The data indicate that IHP binds to HbCO and 785 alters the conformation of the  $\alpha_1\beta_2$ -interface region (i.e., the 786 quaternary structure) and thus could affect the ligand-binding 787 affinity. 788

## 4. FUNCTION

The chief physiological function of Hb is to transport oxygen 789 molecules from the lungs to the tissues of air-breathing 790 vertebrates. This process is affected by a number of factors, e.g., 791 the pH (known as the Bohr effect), allosteric effectors (e.g., 792 hydrogen ions, carbon dioxide, 2,3-BPG, IHP, chloride, and 793 phosphate), and temperature. For a review of the physiological 794 properties of Hb A and mutant Hbs in patients, see Bunn and 795 Forget.<sup>101</sup> 796

### 4.1. Effects of Hydrogen Ions and Allosteric Effectors on Oxygen Affinity

Figure 10 (taken from Figure 4A of ref 12) shows the 798 f10 oxygenation of Hb A in 0.1 M sodium phosphate as a function 799 of pH and in the absence and presence of 5 mM 2,3-BPG or 1 800 mM IHP at 29 °C. The sigmoidal O<sub>2</sub>-binding curves and their 801 dependence on pH and allosteric effectors illustrate the 802 fundamental functional properties of hemoglobin that facilitate 803 the loading and unloading of O<sub>2</sub> molecules efficiently in the 804 physiological system. The O<sub>2</sub> affinity increases in going from 805 pH 6.3 to 7.9. This is known as the alkaline Bohr effect. This 806 effect is important for the ability of Hb to load O<sub>2</sub> in the lungs 807 at higher pH and deliver it to tissues, particularly in working 808 muscles, where lactic acid and CO<sub>2</sub> are produced and the pH is 809 lower. However, the O<sub>2</sub> affinity of Hb A increases again when 810 going from pH 6.3 to 5.7, which is known as the acid Bohr 811 effect. The Bohr effect can be measured by two classical 812 techniques: (i) the difference between the H<sup>+</sup> ion binding 813 curves of HbO<sub>2</sub> (or HbCO) and deoxy-Hb and (ii) the change 814 in O<sub>2</sub> affinity as a function of pH. According to Wyman's 815 linkage relationship, there is an exact relationship between the 816 change in O<sub>2</sub> affinity and the number of H<sup>+</sup> ions released as a 817 function of pH.<sup>102</sup> The maximum number of H<sup>+</sup> ions released 818 per O<sub>2</sub> molecule bound is ~0.5 at pH ~7.4 under physiological 819 conditions. The difference in the number of H<sup>+</sup> ions released or 820 absorbed is due to a change in the pK values of several amino 821 acid residues in the Hb molecule in going from the deoxy to the 822 liganded state. There are two schools of thought regarding the 823 molecular basis of the Bohr effect.<sup>103</sup> One believes that there 824 are only a limited number of amino acid residues involved (e.g., 825 2 to 3 per  $\alpha\beta$  dimer) as proposed by Perutz based on his 826 allosteric mechanism for Hb.<sup>104</sup> The other believes that any 827

758 gives a summary of the water–amide proton exchange rates of  
 759 HbCO A with and without the presence of IHP.<sup>74</sup> Only about  
 760 10% of the amides show relatively large exchange rates. These  
 761 amides are distributed in the N-terminal region, AB  
 762 connections ( $\alpha$ 19Ala– $\alpha$ 20His and  $\beta$ 18Val– $\beta$ 19Asn),  $\alpha$ CD– $\beta$ CE  
 763 loop ( $\alpha$ 44Pro– $\alpha$ 52Ser and  $\beta$ 41Phe– $\beta$ 52Asp), EF loop ( $\alpha$ 72His–  
 764  $\alpha$ 81Ser and  $\beta$ 78Leu– $\beta$ 87Thr), and GH loop ( $\alpha$ 114Pro–  
 765  $\alpha$ 117Phe and  $\beta$ 118Phe– $\beta$ 122Phe). These results illustrate that  
 766 the N-termini and all the loops on both  $\alpha$ - and  $\beta$ -chains are  
 767 dynamic on the millisecond to second time scale.  $\alpha$ 38Thr is  
 768 located in the  $\alpha_1\beta_2$  interface but exhibits a large exchange rate

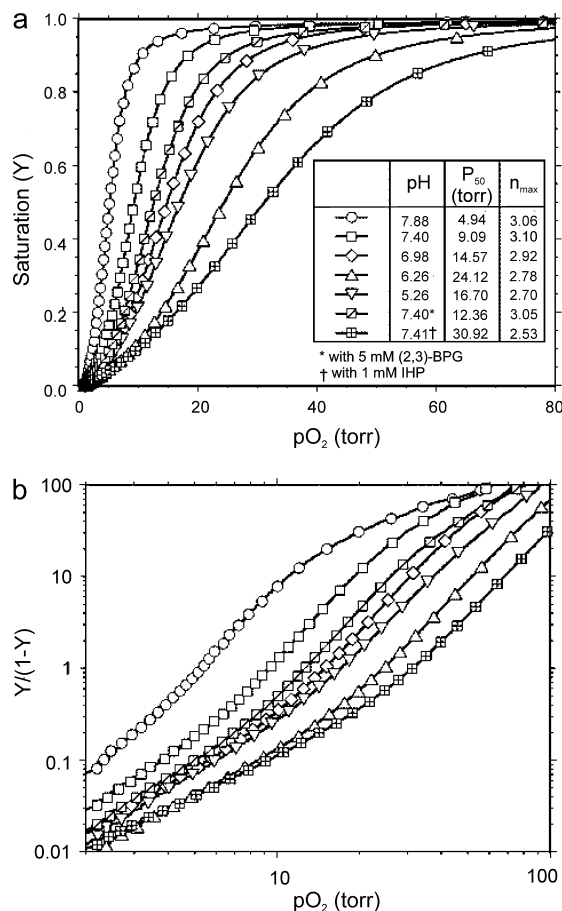


**Figure 10.** (a) Oxygen-binding curves of Hb A measured in 0.1 M phosphate buffer at 29 °C at various pH values in the absence of allosteric effectors and in the presence of 5 mM 2,3-BPG (pH 7.40) or 1 mM IHP (pH 7.41). (b) Hill plots with values calculated according to the corresponding binding curves shown in a. Reprinted with permission from ref 12. Copyright 2004 American Chemical Society.

828 amino acid residue can contribute to the Bohr effect if there is a  
 829 conformational change of that amino acid residue in going from  
 830 the deoxy to the liganded state, i.e., if the pK value of that  
 831 amino acid residue in Hb depends on its environment. In other  
 832 words, the pK values of a large number of amino acid residues  
 833 in Hb can change in going from the deoxy to the oxy (or CO)  
 834 form, and these residues contribute to the Bohr effect,  
 835 positively or negatively. In addition, the amino acid residues  
 836 that have a differential affinity for anions (e.g., chloride,  
 837 phosphate, or 2,3-BPG) can influence the Bohr effect of the Hb  
 838 molecule (known as the anion Bohr effect). On the basis of  
 839 their pK values, the following three types of moieties are  
 840 potential Bohr groups: (i) the imidazoles of His residues, (ii)  
 841 the  $\alpha$ -amino groups from the N-termini, and (iii) other proton-  
 842 binding sites whose pK values are shifted from their normal  
 843 values in the physiological pH range due to their unique  
 844 environments in the Hb molecule. In Hb A, there are 38 His  
 845 residues and 26 of them are located on the surface of the  
 846 molecule;<sup>1</sup> thus, they are likely involved in the Bohr effect.  
 847 <sup>1</sup>H NMR spectroscopy is an excellent tool to investigate the  
 848 contribution of the 26 surface His residues to the Bohr effect  
 849 because the resonances of the C2 protons of the His residues  
 850 can be resolved from other proton resonances and are sensitive  
 851 to the protonation state of the His residues. Using the site-  
 852 directed mutagenesis technique to convert specific His residues

to Gln or Ser, the resonances of the C2 protons of these 26 His residues were assigned and their respective pK values in the deoxy and CO states were determined.<sup>12,105–108</sup> Our experimental results carried out in 0.1 M HEPES plus 0.1 M chloride at 29 °C can be summarized as follows (Table 3, taken

**Table 3. pK Values of Histidyl Residues in Deoxy-Hb A and HbCO A in 0.1 M HEPES plus 0.1 M Chloride in D<sub>2</sub>O at 29 °C<sup>a</sup>**

site	pK (CO)	pK (deoxy)
$\alpha$ 20	7.08 ± 0.01	7.02 ± 0.01
$\alpha$ 45	6.12 ± 0.02	5.25 ± 0.15
$\alpha$ 50	6.90 ± 0.02	7.14 ± 0.01
$\alpha$ 72	7.27 ± 0.01	7.47 ± 0.01
$\alpha$ 89	6.25 ± 0.03	6.80 ± 0.01
$\alpha$ 112	7.53 ± 0.01	7.49 ± 0.01
$\beta$ 2	6.39 ± 0.01	6.17 ± 0.02
$\beta$ 77	7.79 ± 0.01	7.46 ± 0.01
$\beta$ 97	7.75 ± 0.02	8.01 ± 0.01
$\beta$ 116	6.13 ± 0.05	6.35 ± 0.04
$\beta$ 117	6.39 ± 0.02	6.43 ± 0.07
$\beta$ 143	5.57 ± 0.06	4.70 ± 0.05
$\beta$ 146	6.42 ± 0.03	7.93 ± 0.02

<sup>a</sup>Reprinted with permission from ref 12. Copyright 2004 American Chemical Society.

from Table 1 of ref 12): (i) With the exception of  $\alpha$ 20His,  $\alpha$ 112His, and  $\beta$ 117His, the other 23 His residues make very substantial contributions to the observed Bohr effect; (ii) the largest contribution to the alkaline Bohr effect is due to  $\beta$ 146His, while  $\alpha$ 45His and  $\beta$ 143His make the largest contribution to the acid Bohr effect; (iii) several His residues (e.g.,  $\beta$ 2His and  $\beta$ 77His) make negative contributions to the alkaline Bohr effect; (iv) the sum of the contributions from the 26 His residues agrees well with the net measured acid Bohr effect but does not account for the measured alkaline Bohr effect because there must be contributions from other amino acid residues, e.g., the N-terminal residues.<sup>109</sup> For details see Table 3 and Figure 11a (taken from Table 1 and Figure 5, respectively, of ref 12). Another important finding is that the pK values of several His residues are very sensitive to the presence of various anions and the ionic strength.<sup>105,107</sup> Figure 12a and 12b (taken from Figures 2 and 3, respectively, of ref 105) illustrates clearly the effects of buffer and 2,3-BPG on the Bohr effect of Hb A. For example, the pK values for  $\beta$ 2His in deoxy-Hb A vary from 5.83 in 0.1 M HEPES plus 0.1 M chloride to 7.13 in 0.1 M Bis-Tris plus 2,3-BPG, and the corresponding values are 6.24 and 6.68 for HbCO A. The pK values of  $\beta$ 146His in deoxy-Hb A vary from 8.00 in 0.1 M HEPES plus 0.1 M chloride to 8.12 in 0.1 M Bis-Tris plus 2,3-BPG, and the corresponding values for  $\beta$ 146His in HbCO A are 6.24 and 6.68. Figure 13 (taken from Figure 11 of ref 107) shows the change in free energy of proton dissociation for some of the surface histidyl residues upon Hb oxygenation. It demonstrates clearly that the contribution of surface His residues to the Bohr effect is buffer dependent. These results show that the Bohr effect, a heterotropic effect, depends on the detailed environment and interactions of each His residue with its neighbors in the Hb molecule. Thus, the Bohr effect is an excellent example of a global network of electrostatic interactions, rather than a few specific amino acid residues,

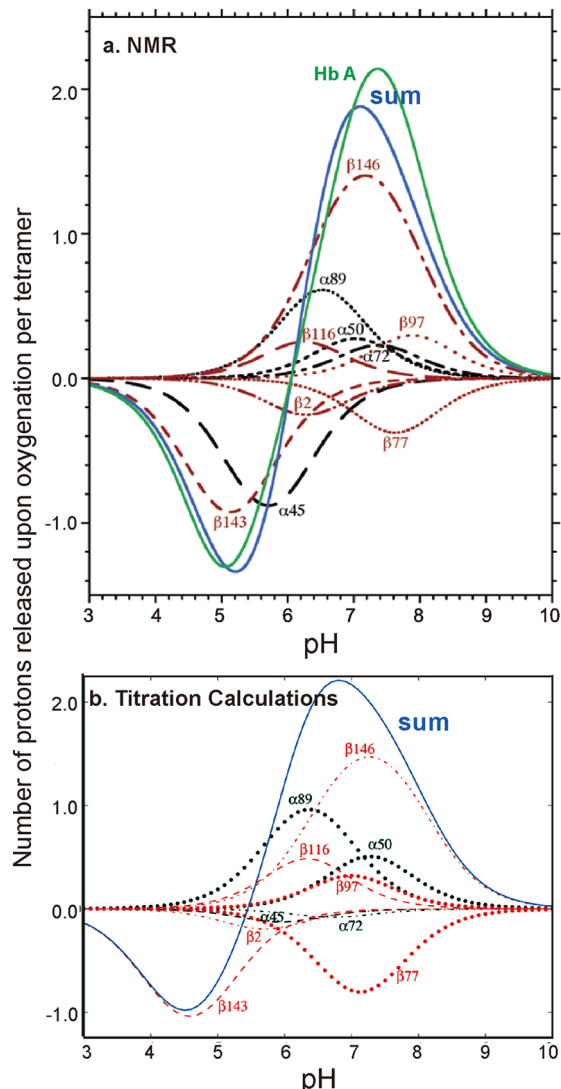


**Figure 11.** (a) Net Bohr effect of Hb A (green) determined from oxygen dissociation studies. Contributions of individual histidyl residues are calculated from pK values determined by NMR spectroscopy. Contributions from 26 surface histidyl residues are represented with the blue line. Reprinted with permission from ref 12. Copyright 2004 American Chemical Society. (b) Contributions of histidyl residues to the Bohr effect of Hb A. Values were calculated based on crystal structures (titration calculations). Contributions of  $\alpha_{20}\text{His}$ ,  $\alpha_{112}\text{His}$ , and  $\beta_{117}\text{His}$  are negligible and not shown. The blue line represents the combined contribution from all 26 surface histidyl residues. Reprinted with permission from ref 110. Copyright 2013 American Chemical Society.

893 playing a dominant role in regulating the physiological function  
894 of Hb A.

895 Karplus and co-workers<sup>110</sup> developed a new computational  
896 method to investigate the “atomic origin” of the Bohr effect of  
897 Hb A. Their method is based on determining the electrostatic  
898 interactions between amino acid residues in crystals of Hb A,  
899 relative to those residues in solution, by use of the linearized  
900 finite difference Poisson–Boltzmann equation and Monte  
901 Carlo sampling of the protonation states. On the basis of the  
902 structural information available from the high-resolution  
903 structures of Hb A in deoxy and CO (or oxy) forms, they  
904 calculated pK values of the His and other residues (in the  
905 absence of 2,3-BPG) and compared them with our NMR

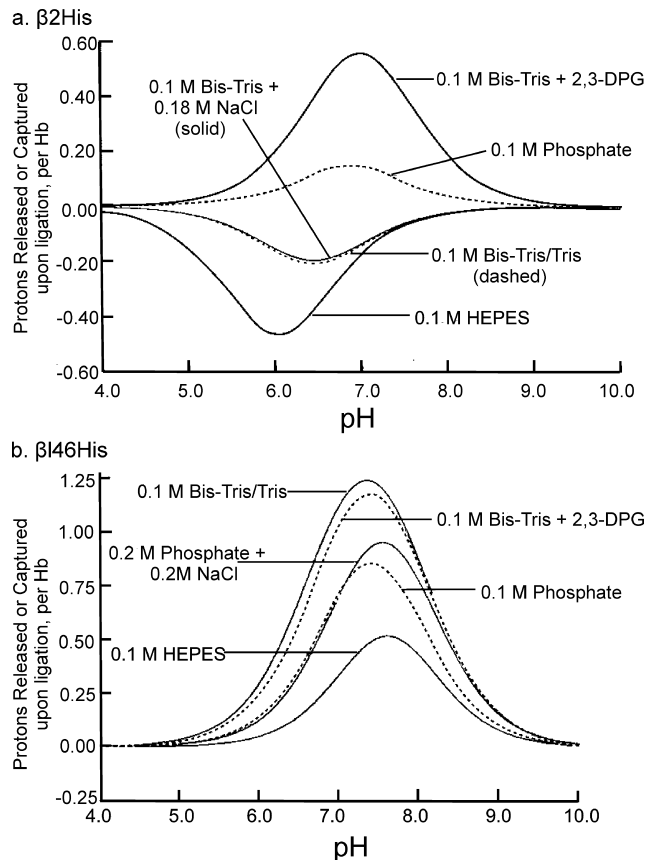


**Figure 12.** (a) Protons released or captured by  $\beta_2\text{His}$  upon Hb A oxygenation. Values were calculated from pH values obtained under various buffers as indicated in the figure. (b) Protons released by  $\beta_{146}\text{His}$  residues upon Hb A oxygenation. Values were calculated from pK values obtained under experimental conditions as indicated in the figure. Reprinted with permission from ref 105. Copyright 1990 Elsevier.

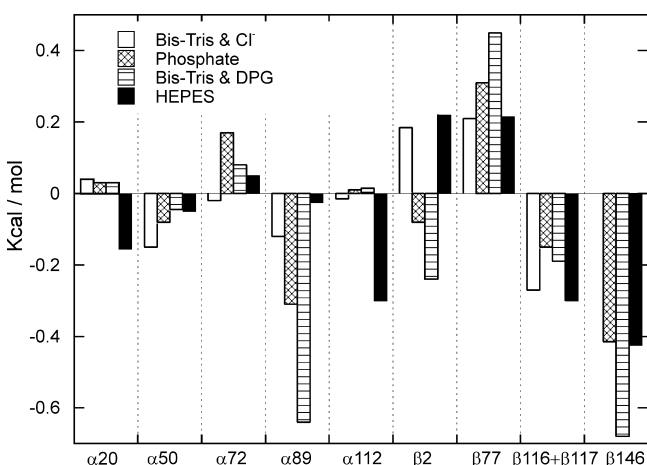


**Figure 13.** Change in proton dissociation energy of surface histidines upon Hb A oxygenation under various buffer conditions. Adapted with permission from ref 107. Copyright 1997 American Chemical Society.

906 results for the His residues. Tables 4 and 5 (taken from Tables 906 t4t5  
907 4 and 5 of ref 110) give both their calculated and our 907  
908 experimentally determined values. Structures 2DN2 (for deoxy) 908  
909 and 2DN3 (for oxy) with the highest resolution were used in 909  
most of their analyses. They reported that the magnitude of the 910

**Table 4.** His pK<sub>a</sub> Values in Deoxy-Hb Determined by NMR and Calculated from Several T-Type Crystal Structures Using Minimized WHATIF Structures, and Absolute Deviations (numbers in parentheses) of the Calculated Values from the Experimental Values<sup>a</sup>

subunit	ResID	NMR	2DN2	4HBB	1BZ0	1RQ3	1XXT	1KD2
α	20	7.02	<b>6.14 [0.88]</b>	7.11 [0.09]	6.93 [0.09]	6.95 [0.07]	6.95 [0.07]	6.78 [0.24]
α	45	5.25	<b>5.88 [0.63]</b>	5.90 [0.65]	5.85 [0.60]	5.64 [0.39]	5.56 [0.31]	6.01 [0.76]
α	50	7.14	<b>7.50 [0.36]</b>	7.35 [0.21]	7.30 [0.16]	7.15 [0.00]	7.21 [0.07]	7.05 [0.09]
α	58		<b>4.33</b>	4.54	4.06	3.54	3.79	4.55
α	72	7.47	<b>6.69 [0.78]</b>	6.67 [0.80]	6.72 [0.75]	6.89 [0.59]	6.74 [0.73]	6.68 [0.80]
α	87		<b>2.95</b>	3.05	3.28	3.45	3.89	3.43
α	89	6.80	<b>6.82 [0.02]</b>	6.78 [0.02]	6.46 [0.34]	6.82 [0.02]	6.77 [0.03]	6.54 [0.26]
α	103		<b>3.92</b>	4.19	3.58	3.60	3.55	4.37
α	112	7.49	<b>6.64 [0.85]</b>	6.93 [0.56]	6.66 [0.83]	6.60 [0.89]	6.89 [0.60]	6.84 [0.65]
α	122		<b>0.53</b>	0.64	0.78	0.99	0.82	1.08
β	2	6.17	<b>5.61 [0.56]</b>	5.51 [0.66]	5.27 [0.90]	4.97 [1.20]	5.12 [1.05]	5.70 [0.47]
β	63		<b>4.93</b>	5.30	4.84	5.69	4.82	3.85
β	77	7.46	<b>6.76 [0.70]</b>	6.70 [0.76]	6.89 [0.57]	6.92 [0.54]	6.83 [0.63]	7.05 [0.41]
β	92		<b>3.61</b>	3.70	3.56	3.22	3.14	3.73
β	97	8.01	<b>7.13 [0.88]</b>	7.26 [0.75]	7.02 [0.99]	7.12 [0.89]	7.04 [0.97]	7.04 [0.97]
β	116	6.35	<b>6.55 [0.20]</b>	6.64 [0.29]	6.36 [0.01]	5.71 [0.64]	5.62 [0.73]	6.74 [0.39]
β	117	6.43	<b>8.01 [1.58]</b>	8.11 [1.68]	7.44 [1.01]	7.57 [1.14]	7.77 [1.34]	6.28 [0.15]
β	143	4.70	<b>4.08 [0.62]</b>	3.85 [0.85]	4.52 [0.19]	4.82 [0.12]	4.69 [0.02]	4.82 [0.12]
β	146	7.93	<b>8.08 [0.15]</b>	7.58 [0.35]	7.86 [0.07]	7.84 [0.09]	7.81 [0.12]	8.12 [0.19]
max error			[1.58]	[1.68]	[1.01]	[1.20]	[1.34]	[0.97]
ave. error			[0.63]	[0.59]	[0.50]	[0.51]	[0.51]	[0.42]

<sup>a</sup>Reprinted with permission from ref 110. Copyright 2013 American Chemical Society.

**Table 5.** His pK Values of Liganded Hb A Determined by NMR and Calculated from the Crystal Structure Using Minimized WHATIF Structures, and Deviations (numbers in parentheses) of the Calculated Values from the Experimental Values<sup>a</sup>

subunit	ResID	NMR	2DN3	1HHO(R)	1BBB(R2)	1MKO(RR2)	1YZI(R3)
α	20	7.08	<b>7.15 [0.07]</b>	7.18 [0.10]	7.05 [0.03]	7.18 [0.10]	7.03 [0.05]
α	45	6.12	<b>5.99 [0.14]</b>	5.86 [0.26]	6.14 [0.02]	6.24 [0.12]	6.46 [0.34]
α	50	6.90	<b>7.05 [0.15]</b>	7.04 [0.14]	7.40 [0.50]	7.28 [0.38]	7.26 [0.36]
α	58		<b>3.88</b>	3.55	5.00	4.40	5.04
α	72	7.27	<b>6.76 [0.51]</b>	6.58 [0.69]	6.68 [0.59]	6.82 [0.45]	6.72 [0.55]
α	87		<b>3.71</b>	3.16	3.69	3.09	3.01
α	89	6.25	<b>5.91 [0.34]</b>	5.92 [0.33]	7.12 [0.87]	5.80 [0.45]	5.67 [0.59]
α	103		<b>3.17</b>	2.79	3.99	2.41	3.94
α	112	7.53	<b>7.20 [0.33]</b>	5.80 [1.73]	6.24 [1.29]	6.66 [0.87]	6.22 [1.32]
α	122		<b>0.79</b>	1.04	0.77	0.19	1.34
β	2	6.39	<b>5.78 [0.61]</b>	5.84 [0.55]	5.93 [0.46]	5.99 [0.40]	6.77 [0.38]
β	63		<b>5.89</b>	5.70	6.43	5.69	5.62
β	77	7.79	<b>7.50 [0.29]</b>	7.33 [0.46]	7.14 [0.65]	7.39 [0.40]	6.25 [1.54]
β	92		<b>4.58</b>	4.30	3.53	4.21	5.25
β	97	7.75	<b>6.85 [0.90]</b>	7.01 [0.74]	6.77 [0.98]	6.77 [0.98]	7.62 [0.13]
β	116	6.13	<b>6.12 [0.01]</b>	6.33 [0.20]	6.73 [0.60]	6.81 [0.68]	7.16 [1.03]
β	117	6.39	<b>6.35 [0.04]</b>	6.05 [0.34]	5.87 [0.52]	6.21 [0.18]	6.80 [0.41]
β	143	5.57	<b>5.08 [0.49]</b>	4.75 [0.82]	5.43 [0.14]	4.89 [0.68]	2.29 [3.28]
β	146	6.42	<b>6.45 [0.03]</b>	2.24 [4.18]	1.30 [5.12]	5.31 [1.11]	4.58 [1.84]
max error			[0.90]	[4.18]	[5.12]	[1.11]	[3.28]
ave. error			[0.30]	[0.81]	[0.91]	[0.52]	[0.91]

<sup>a</sup>All structures are for HbCO A, except 1HHO, which is for oxy-Hb A. Reprinted with permission from ref 110. Copyright 2013 American Chemical Society.

average prediction error is ~0.5 pK unit, and the maximum error is less than 1 pK unit. Figure 11b (taken from Figure 5b of ref 110) gives a plot of the calculated contributions of His residues to the Bohr effect of Hb A, similar to Figure 12a for results obtained from the NMR experiments. The calculated results for the pKs of the His residues provide an excellent opportunity for a comparison with the experimentally

determined pK values for the surface His residues. A major conclusion is that there are many His residues that participate in the Bohr effect, supporting the conclusion derived from our NMR results. However, there are differences between specific pK values determined by NMR in solution and those determined by calculations, depending on which crystal structures were used. As shown in Figures 12 and 13, the pK

925 values of specific His residues and their contributions to the  
926 Bohr effect can vary depending on the solution conditions (e.g.,  
927 buffer, 2,3-BPG, phosphate, chloride, etc.). Since various  
928 crystals were grown under various conditions and the crystals  
929 were frozen for high-resolution X-ray crystallographic experi-  
930 ments, the conformations of some of the His residues can vary  
931 from crystal to crystal, thus giving different pK values in  
932 different crystal structures. A possible way to resolve this matter  
933 is to carry out the calculations using the NMR solution  
934 structure for HbCO A (PDB entry 2M6Z).<sup>74</sup>

935 Both experimentally measured and calculated results show  
936 that  $\beta$ 146His makes the largest contribution to the alkaline  
937 Bohr effect, and its contribution to the Bohr effect is affected by  
938 experimental conditions. However, there are differences in the  
939 pK values of  $\beta$ 146His between these two sets of results (Tables  
940 4 and 5) depending on the crystal structures used in the  
941 calculations and the experimental conditions for the NMR  
942 measurements. The proton resonance assignment for  $\beta$ 146His  
943 in HbCO A and its role in the Bohr effect<sup>105,106,111–120</sup> were  
944 quite challenging and controversial in the 1980s. Figure 14

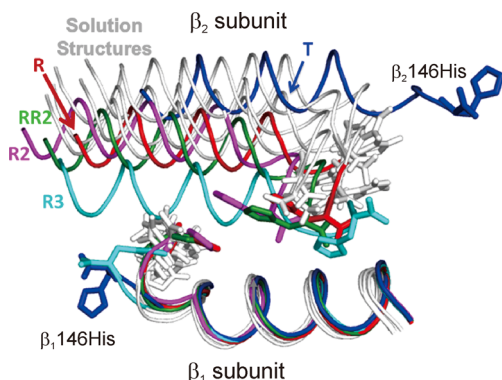


**Figure 14.** Conformations of  $\beta$ 146His in the crystal structures of deoxy-Hb A (2DN2, blue), HbCO A in R (2DN3, red), R2 (1BBB, magenta), RR2 (1MKO, green), and R3 (1YZI, cyan) forms and the five lowest energy NMR structures (2M6Z, light gray). Structures are superimposed on the backbones of the  $\beta_1$ -subunits. Side chains of  $\beta$ 146His are presented as sticks. Figures were generated with the PyMOL program.<sup>61</sup>

945 shows that there are many conformations for  $\beta$ 146His in the  
946 solution structures of HbCO A, and they are distinct from the  
947 crystal structures. This could account for the early difficulties in  
948 obtaining the correct spectral assignment for this His residue in  
949 HbCO A, thus leading to the controversies concerning its role  
950 in the alkaline Bohr effect of Hb A. However, the role of  
951  $\beta$ 146His in the Bohr effect was established once its correct  
952 resonance assignment was made.<sup>105,106,116</sup>

953 In addition, Karplus and co-workers also provided the  
954 contributions of  $\alpha$ 1Val to the Bohr effect.<sup>110</sup> Their calculated  
955 pK values for the N-terminal  $\alpha$ 1Val are 8.60 and 7.80 for deoxy-  
956 and oxy-Hb A, respectively. They found that the number of  
957 hydrogen ions released from the two  $\alpha$ -chains at pH 8.4 is 0.32,  
958 corresponding to 16% of the Bohr effect at that pH.<sup>116</sup>

959 On the basis of the NMR and computation studies, we can  
960 conclude that (i)  $\beta$ 146His plays a very large role in the alkaline  
961 Bohr effect of Hb A and its contribution depends on buffer  
962 conditions, (ii)  $\alpha$ 58His and  $\beta$ 143His are responsible for the  
963 acid Bohr effect, and (iii) in addition to  $\beta$ 146His the other 24  
964 surface His residues plus  $\alpha$ 1Val also make significant  
965 contributions (~30%) to the alkaline Bohr effect of Hb A.<sup>105</sup>

## 4.2. Effect of Temperature on Oxygen Affinity

Because Hb oxygenation is exothermic, the  $O_2$  affinity decreases markedly with increasing temperature and increases with decreasing temperature. For heterothermic mammals, this feature of Hb may pose considerable challenges for  $O_2$  delivery to cool extremities and peripheral tissues. Recently,<sup>121–123</sup> a smaller temperature effect on oxygen binding has been found for the recombinant woolly mammoth Hb (rHb WM) compared to the Asian elephant Hb (rHb AE). Elephants are a particularly good model system to investigate the effects of temperature on the structure–function relationship of Hb as they include both warm- and cold-adapted members.<sup>976</sup>

The primary sequence of Asian elephant Hb differs from that of the mammoth at only one position in the  $\alpha$ -globin chain (KSN) and at three positions (T12A, A86S, and E101Q) in the  $\beta/\delta$ -fusion globin chain.  $\beta/\delta$ 101Gln is located between  $\beta/\delta$ 99Asp and  $\beta/\delta$ 102Asn of the same chain in the intersubunit  $\alpha_1(\beta/\delta)_2$  interface. These residues are all critical to the function of Hb. rHb WM and the human mutant Hb Rush,<sup>124</sup> both having Gln at the  $\beta$ 101 position, are affected similarly by chloride ions. rHb WM exhibits a more significant effect of chloride on the  $O_2$  affinity than rHb AE, as does Hb Rush compared to Hb A. Thus, Campbell et al.<sup>121</sup> suggested that the  $\beta/\delta$ 101Gln in rHb WM is responsible for the lower temperature effect by providing additional binding sites for chloride in the central cavity of the Hb molecule. However, X-ray structural analyses<sup>125–127</sup> have not shown the specific binding sites for chloride ions in woolly mammoth Hb, Hb A, or bovine Hb. Further, the studies of rHb WM and a number of its mutants created at the  $\beta/\delta$ 101 position, with special reference to Hb A, have shown that chloride can alter the temperature dependence of  $O_2$  binding, in addition to its allosteric role in regulating the  $O_2$  affinity of hemoglobin.<sup>123</sup> A more significant decrease of the temperature effect of rHb WM and its mutants is observed in the presence of both chloride and IHP, two allosteric effectors which both lower the affinity for  $O_2$ . The amino acid residue  $\beta$ 101 is one example that a specific residue could be responsible for the effect of temperature on oxygen affinity. If the replacement of certain amino acid residues in the Hb molecule could cause a stronger response to allosteric effectors, it is possible that those mutant Hbs could exhibit a lower temperature effect. This is an interesting proposition.<sup>1007</sup>

## 4.3. Oxygen Affinity Related to the Distal Hydrogen Bond

On the basis of X-ray crystal structures and electron paramagnetic resonance and resonance Raman spectroscopic measurements,<sup>128,129</sup> it was proposed that  $O_2$  binding to hemoglobin is stabilized by hydrogen bonds between the oxygen ligand and the side chain of the two distal histidyl residues,  $\alpha$ 58His and  $\beta$ 63His. Our study by multinuclear NMR provided the first direct evidence of such H bonds in  $HbO_2$  A in solution.<sup>130</sup> The cross-peaks for the side chains of  $\alpha$ 58His and  $\beta$ 63His in NMR spectra can be used as markers to demonstrate the strength of the H bonds, which have been observed for Hb A and five mutant rHbs.<sup>131</sup> The changes in these markers are correlated with the effect of pH and/or temperature on the  $O_2$ -binding affinity, and this relationship is demonstrated by the weakening and even the disappearance of the cross-peaks in the NMR spectra under conditions where the affinity decreases. At higher pH and/or lower temperature, the cross-peaks for both  $\alpha$ 58His ( $^1\text{He}_2$ ,  $^{15}\text{Ne}_2$ ) and  $\beta$ 63His ( $^1\text{He}_2$ ,  $^{15}\text{Ne}_2$ ) are clearly visible in Figure 15 (taken from Figure 2 of f15).

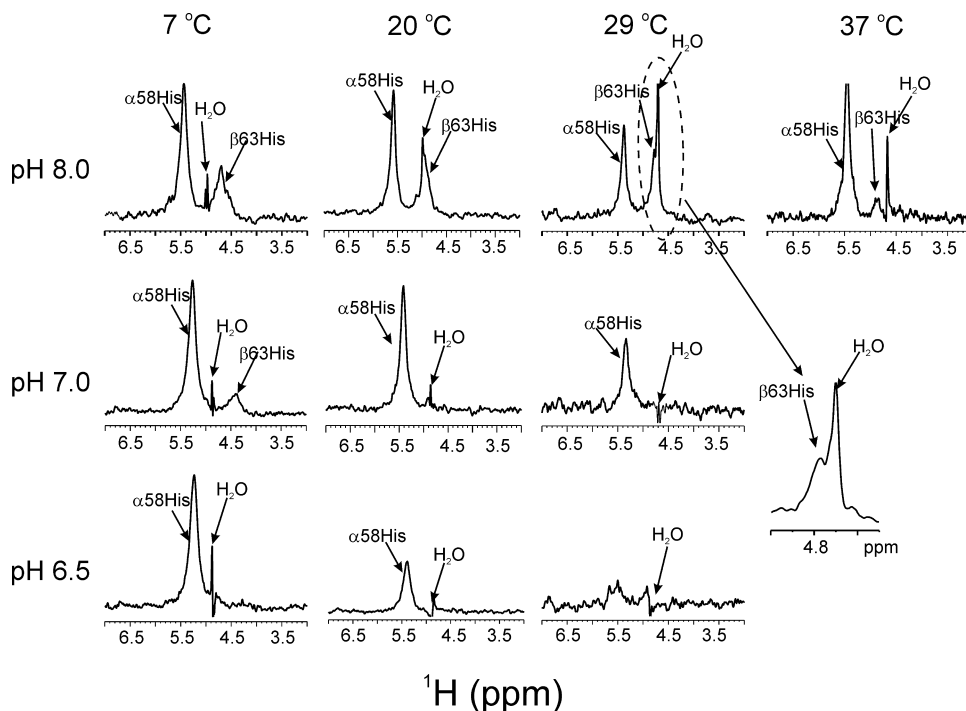


**Figure 15.** Horizontal 1D slices along the  $^1\text{H}$  axis through the cross-peak of the  $\beta$ 63His side chain. Data were extracted from 600 MHz ( $^1\text{H}, ^{15}\text{N}$ ) HSQC spectra of fully  $^{15}\text{N}$ -labeled rHbO<sub>2</sub> A in  $\text{H}_2\text{O}$  under various conditions of pH and temperature. Adapted with permission from ref 131. Copyright 2010 American Chemical Society.

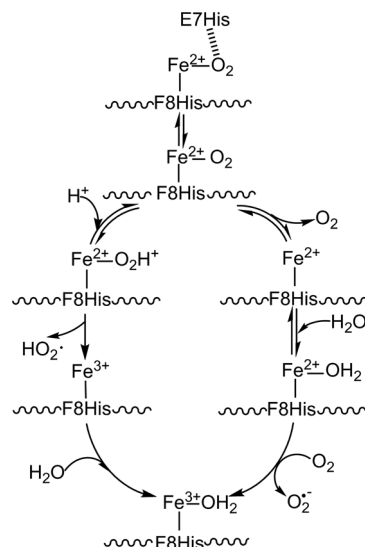
ref 131). When pH is decreased and/or at higher temperature, the side chains of the distal histidines appear to be more mobile, and the exchange with water molecules in the distal heme pockets is faster. Consequently, the cross peaks lose intensity or even disappear. These H-bond markers in the NMR spectra can also show subtle differences between the distal heme pockets of the  $\alpha$ - and  $\beta$ -chains of Hb A. The H bond in the heme pocket of the  $\beta$ -chain is weaker than that in the  $\alpha$ -chain and more sensitive to changes in pH and temperature. IHP has only a minor effect on these H-bond markers compared to the effects of pH and temperature. These H bonds are found to be sensitive to mutations in the distal heme pockets but not affected directly by mutations in the quaternary interfaces, i.e., the  $\alpha_1\beta_1$  and/or  $\alpha_1\beta_2$  subunit interfaces.<sup>131</sup>

#### 4.4. Autoxidation

The Fe atom of the porphyrin heme is covalently bound to the proximal F8His ( $\alpha$ 87His or  $\beta$ 92His) and in close proximity to B10Leu ( $\alpha$ 29Leu or  $\beta$ 28Leu), E7His ( $\alpha$ 58His or  $\beta$ 63His), and E11Val ( $\alpha$ 62Val or  $\beta$ 67Val) of the distal pocket.<sup>1</sup> The importance of these residues has been studied by various groups.<sup>132–143</sup>

The heme-iron atom can undergo autoxidation and convert from the ferrous ( $\text{Fe}^{2+}$ ) to the ferric ( $\text{Fe}^{3+}$ ) state.<sup>144</sup> The  $\text{Fe}^{2+}$  form of the heme-iron cannot bind oxygen, and Hb A is inactivated when all four iron atoms of the tetramer are oxidized to form met-Hb, resulting in an increased rate of hemin loss and eventual denaturation of the apoglobin.<sup>145</sup> This process has been studied extensively using myoglobin (Mb) as a model system.<sup>146–150</sup> The reaction initiates by weakening the H bond between the bound oxygen and the Ne atom of the E7His. From this point on, there are two proposed mechanisms for the reaction, summarized in Scheme 1. The  $\text{Fe}^{2+}\text{O}_2$  complex is first protonated. The hydroperoxyl

#### Scheme 1. Possible Mechanism of Hb A Autoxidation<sup>a</sup>



<sup>a</sup>Schematic presentation of reactions in converting the heme-iron atom from the ferrous ( $\text{Fe}^{2+}$ ) to the ferric ( $\text{Fe}^{3+}$ ) state. Scheme adapted from ref 147. Copyright 1993 American Society for Biochemistry and Molecular Biology.

radical ( $\text{HO}_2^\bullet$ ) then dissociates from the protein and leaves behind an  $\text{Fe}^{3+}$  ion for reacting with water to form aquomet-Mb. Alternatively, the oxygen dissociates from the heme and allows the  $\text{Fe}^{2+}$  ion of the deoxy-Mb to interact with water. The aquo-Mb and free oxygen then undergo a bimolecular reaction to form aquomet-Mb and the superoxide radical ( $\text{O}_2^\bullet-$ ). In addition, the autoxidation reaction is an acid-catalyzed process<sup>147,151,152</sup> and can be promoted by anions such as azide.<sup>136,142,150,153</sup> The imidazole ring of the E7His possibly

1068 facilitates the movement of a proton from the solvent to the  
1069 bound oxygen.<sup>151</sup> Park et al.<sup>35</sup> identified occupied water  
1070 molecules in the distal heme pockets of the  $\alpha$ -subunits of  
1071 oxy-Hb A. These water molecules could facilitate the  
1072 autoxidation process and explain the observation that the  $\alpha$ -  
1073 chain ( $0.032 \text{ h}^{-1}$ ) can oxidize more rapidly than the  $\beta$ -chain  
1074 ( $0.0037 \text{ h}^{-1}$ ) in the Hb A tetramer at pH 7.2 in an early  
1075 report.<sup>154</sup> A less dramatic difference between the autoxidation  
1076 rate of the  $\alpha$ - ( $0.078 \text{ h}^{-1}$ ) and  $\beta$ -chains ( $0.011 \text{ h}^{-1}$ ) at pH 6.5  
1077 was reported by Tsuruga et al.<sup>144,152</sup>

1078 We substituted other amino acids for B10Leu and E11Val  
1079 and gauged the effects on autoxidation or azide-induced  
1080 oxidation.<sup>136,142,153,155</sup> The results are summarized in Table 6.

**Table 6. Autoxidation Rate and Oxygen Binding Properties of Hb A and Recombinant Heme-Pocket Mutants<sup>a</sup>**

	$k_{\text{ox}}^b$	$k_{\text{az}}^b$	$P_{50} \text{ mm Hg (pH 7.4)}$	ref
Hb A	1	1	8.0	136 <sup>c</sup>
rHb( $\alpha$ L29F)	0.47	0.36	4.0	
rHb( $\alpha$ L29F,V96W/ $\beta$ N108 K)	1.29	0.59	22	
Hb( $\alpha$ V96W/ $\beta$ N108 K)	3.8	1.6	38.1	
rHb( $\beta$ N108Q)	2.84	n.d.	17.5	155 <sup>d</sup>
rHb( $\alpha$ L29F/ $\beta$ N108Q)	1.16	n.d.	12.1	
rHb( $\alpha$ L29F,V96W/ $\beta$ N108 K)	2.84	n.d.	n.d.	
rHb( $\alpha$ L29F)	1	0.23	4.9	153 <sup>c</sup>
rHb( $\alpha$ L29W)	7.7	1.2	31.5	
rHb( $\beta$ L28F)	18.9	1.7	35.7	
Hb( $\beta$ L28W)	21.1	4.0	64.6	
rHb( $\alpha$ V62L)	4.6	2.3	7.5	142 <sup>c</sup>
rHb( $\alpha$ V62I)	3.1	0.9	9.0	
rHb( $\alpha$ V62F)	5.5	3.0	7.2	
rHb( $\beta$ V67L)	4.4	2.5	7.5	
rHb( $\beta$ V67I)	3.8	1.3	18.2	
rHb( $\beta$ V67F)	6.8	3.6	2.7	

<sup>a</sup>Data from refs 136, 142, 153, and 155. <sup>b</sup> $k_{\text{ox}}$  and  $k_{\text{az}}$  results are normalized to that of Hb A. <sup>c</sup> $k_{\text{ox}}$  results determined in 0.1 M phosphate and 1 mM EDTA, pH 7.0 at 25 °C. <sup>d</sup> $k_{\text{ox}}$  results determined in PlasmaLyte buffer, pH 7.4 and 37 °C. n.d., not determined.

1081 Substituting a bulky aromatic side chain for B10Leu or E11Val  
1082 can reduce the capture volume in the distal pocket and possibly  
1083 exclude water from the  $\alpha$ -subunit heme pocket.<sup>133,134</sup>  
1084 Replacement of E11Val also removes the  $\gamma_2$ -methyl group  
1085 that provides steric hindrance to access the heme Fe.<sup>133</sup>  
1086 Therefore, E11Val mutants, in general, have higher  $k_{\text{ox}}$  and  $k_{\text{az}}$   
1087 values.<sup>142</sup> Among the B10 and E11 mutants,<sup>136,153,155</sup> only rHb  
1088 ( $\alpha$ L29F) has  $k_{\text{az}}$  lower than Hb A. Jeong et al.<sup>136</sup> reported that  
1089 the  $k_{\text{ox}}$  of rHb ( $\alpha$ L29F) was also lower than that of Hb A and  
1090 gave the reason that the positive edge of the phenyl ring  
1091 multipole might stabilize the bound oxygen.<sup>134</sup> However, this  
1092 lowering in  $k_{\text{ox}}$  has not been detected by Wiltrot et al.<sup>153</sup> or  
1093 Tam et al.<sup>142</sup>

1094 The factors determining the autoxidation process are mainly  
1095 (i) the stability of the H bond between the bound oxygen and  
1096 E7His and (ii) the stereoplacement of E7His, B10Leu, and  
1097 E11Val controlling the entry of reactant (water, oxygen, or  
1098 azide) into the distal pockets. It is of interest to note that the H  
1099 bond between the bound oxygen and E7His in the  $\beta$ -subunit is  
1100 weaker than that in the  $\alpha$ -subunit,<sup>131</sup> while the  $\beta$ -subunit has  
1101 also a slower  $k_{\text{ox}}$ . Therefore, the stereoplacement of amino acid

1102 residues in the heme pocket is the major contributing factor in  
1103 determining the  $k_{\text{ox}}$  of the subunit.<sup>1102</sup>

#### 4.5. Effects of Interfacial and Distal Heme-Pocket Mutations on the Structure and Function of Hemoglobin<sup>1104</sup>

Kinetic and equilibrium studies of ligand binding as well as structural studies with  $^1\text{H}$  NMR have been carried out to investigate recombinant Hb mutants, rHb ( $\alpha$ L29F), rHb ( $\alpha$ L29W), rHb ( $\alpha$ V96W), rHb ( $\beta$ N108 K), rHb ( $\alpha$ V96W/ $\beta$ N108 K), rHb ( $\alpha$ L29F/ $\alpha$ V96W/ $\beta$ N108 K), and rHb ( $\alpha$ L29W/ $\alpha$ V96W/ $\beta$ N108 K).<sup>138</sup> The first two rHbs have single amino acid substitutions at the distal heme pocket of the  $\alpha$ -chain. rHb ( $\alpha$ V96W) and rHb ( $\beta$ N108 K) have a single mutation in the  $\alpha_1\beta_2$  and the  $\alpha_1\beta_1$  interface, respectively. The double mutant, rHb ( $\alpha$ V96W/ $\beta$ N108 K), has mutations in both the  $\alpha_1\beta_2$  and the  $\alpha_1\beta_1$  interfaces. The two triple mutants, rHb ( $\alpha$ L29F/ $\alpha$ V96W/ $\beta$ N108 K) and rHb ( $\alpha$ L29W/ $\alpha$ V96W/ $\beta$ N108 K), have mutations at the distal heme pocket of the  $\alpha$ -chain as well as in both the  $\alpha_1\beta_2$  and the  $\alpha_1\beta_1$  interfaces. These recombinant mutants were used to test the hypothesis that the distal heme-pocket mutations produce only local structural and functional changes at the ligand-binding site, while the mutations in the  $\alpha_1\beta_2$  and  $\alpha_1\beta_1$  interfaces affect the equilibrium between the R and the T quaternary states. We found that the placement of Phe or Trp at the  $\alpha$ 29 position resulted in 40- and 300-fold decreases, respectively, in the rate constant for bimolecular  $\text{O}_2$  binding to the R state  $\alpha$ -chains measured after partial photolysis the  $\text{HbO}_2$  tetramers. In contrast, the rate constants for the wild-type  $\beta$ -chains are relatively unaffected by the mutation in their partner  $\alpha$ -chains. The  $\beta$ N108 K mutation in the  $\alpha_1\beta_1$  interface produces a small slow phase for both  $\text{O}_2$  and CO rebinding after partial photolysis (~25% of the total amplitude). Unlike the distal heme-pocket mutants, this lowered rate constant is not the result of a change in the intrinsic reactivity of the mutated subunit, as is seen for the mutations in the distal heme pocket, but appears to be the result of shifting the tetramer structure toward the T quaternary state. Both liganded rHb ( $\beta$ N108 K) and rHb ( $\alpha$ V96W) can be converted to the T-type structure in fully liganded tetramers<sup>86,156</sup> by lowering the temperature and upon the addition of IHP. The ability to switch the quaternary structure in fully liganded forms<sup>157</sup> is increased when these two mutations are combined in rHb ( $\alpha$ V96W/ $\beta$ N108 K). Both NMR spectra<sup>157</sup> and WAXS pattern<sup>84</sup> suggest that rHb ( $\alpha$ V96W/ $\beta$ N108 K) assumes a conformation intermediate between that of the T and the R forms. Interestingly, the solution structure determined by NMR shows (Figure 14) that some structural elements can span a range of positions in the liganded state (CO) and get close to the deoxy T structure. The rHb ( $\alpha$ L29F) mutant has high  $\text{O}_2$  affinity, while the rHb ( $\alpha$ L29W) variant has low  $\text{O}_2$  affinity. In the triple mutant, rHb ( $\alpha$ L29F/ $\alpha$ V96W/ $\beta$ N108 K), the T to R transition is inhibited by mutating both  $\alpha_1\beta_2$  and  $\alpha_1\beta_1$  interfaces, thus compensating for the intrinsic increase in  $\text{O}_2$  affinity caused by the  $\alpha$ L29F substitution. Conversely, rHb ( $\alpha$ L29W/ $\alpha$ V96W/ $\beta$ N108 K) exhibits a further drastic drop in  $\text{O}_2$  affinity. Results from these mutants confirm that the effects of single distal heme-pocket and interface mutations are additive, and their individual properties can be used to design novel recombinant Hbs with unique properties. For details, see ref 138.

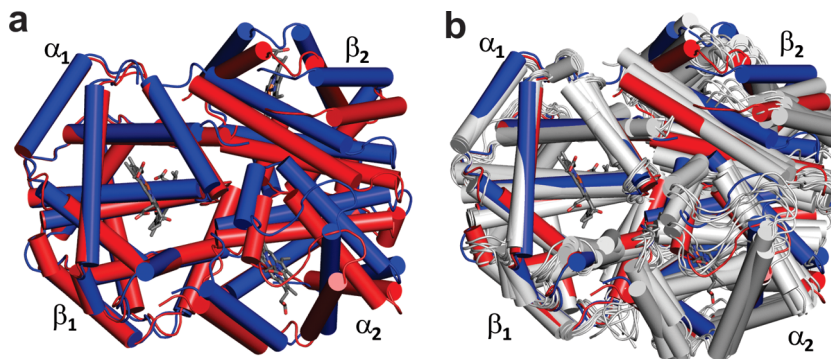


**Figure 16.** Evolving view of hemoglobin allostery from a rigid two-structure model (a) to a dynamic ensemble of the solution structures (b). (a) T(unliganded-form, PDB code 4HHB, blue) and the R (liganded-form, PDB code 2DN3, red) structures of Hb A are superimposed. (b) Ten lowest energy solution structures of HbCO A obtained by NMR (PDB code 2M6Z, gray) are superimposed with the T and R structures of Hb A obtained by X-ray crystallography. Structures are aligned according to the  $\alpha_1\beta_1$  dimer. Figures were generated with the PyMOL program.<sup>61</sup>

## 5. DYNAMIC AND STRUCTURAL BASIS OF HEMOGLOBIN ALLOSTERY

Our recent NMR structural and dynamic studies of Hb A have led to a number of conclusions. (i) Hemoglobin is a flexible and dynamic molecule with a considerable amount of plasticity, exhibiting various types of motions in the backbone and side-chain residues (ranging from picoseconds to nanoseconds and microseconds to milliseconds).<sup>74,81,90,95</sup> (ii) RDC measurements for HbCO A and a low oxygen-affinity mutant Hb, rHb ( $\alpha V96W$ ), in the absence and presence of IHP, have confirmed that the transition pathway<sup>69,70</sup> from the unliganded to the liganded state of hemoglobin is likely T  $\rightarrow$  R  $\rightarrow$  R2. (iii) Allosteric effectors, e.g., IHP, alter both the tertiary and the quaternary structure of deoxy- and CO-Hb as well as the dynamics of the Hb molecule, thus affecting its ligand affinity.<sup>70–72,74</sup> (iv) RDC measurements of Hb A in different aqueous liquid crystalline media and at several magnetic field strengths have shown that in solution the quaternary conformations for both the CO and the deoxy forms of Hb A are different from their crystal structures, and both exist as dynamic ensembles of various structures.<sup>69–72</sup> It is tempting to speculate that the various T- and R-type structures reported by crystallographers (Table 1) may be the so-called “pre-existing protein conformations” and represent some of the conformational ensembles detected by our NMR measurements. Their individual populations can be shifted under different experimental conditions.

Recent experimental and theoretical studies have emphasized the important roles that dynamics and conformational ensembles can play in regulating protein–ligand interactions,<sup>158–167</sup> consistent with the conclusions derived from our structural and dynamic results on Hb presented here. The ensemble nature of Hb structure presents a different picture from the classical two-structure allosteric model of MWC/Perutz or the KNF sequential model based on two quaternary structures, namely, the unliganded (deoxy) (i.e., T type) and liganded (oxy or CO) (i.e., R type) structures. Thus, in this new picture of Hb allostery, we need to consider the statistical nature of various factors that contribute to the cooperative oxygenation process and the roles of allosteric effectors that fine tune the functional properties of hemoglobin under physiological conditions. Our NMR results also illustrate that various parts of the Hb molecule are sensitive to changes in experimental conditions, e.g., partial pressure of O<sub>2</sub> or CO, pH, nature and concentration of buffers, and allosteric effectors,

as well as temperature. Through the use of naturally occurring human mutant hemoglobins as well as of a large number of recombinant mutant Hbs produced by using our Hb expression plasmid, we carried out an extensive array of structural, dynamic, kinetic, and functional studies.<sup>67,81,86,90,96,120,131,138,153,156,168–176</sup> Some of the observed structural, dynamic, kinetic, and functional changes can be related to the mutations. Some of them can be small, but the mutation at one site could affect the conformation of distant as well as neighboring residues. These types of conformational alterations could play significant roles in the structure–function relationship of Hb. An important consequence of an ensemble nature of allosteric interactions is that it could be related to the allosteric coupling process. It should also be recognized that very rapid fluctuations on picosecond or nanosecond time scales give an average kinetic or equilibrium property on longer time scales or at equilibrium. For a discussion on this matter, see Petrich et al.<sup>177</sup> From a mechanistic point of view, we need to know how the structures and dynamics of various amino acid residues of the partially liganded species play out during the cooperative oxygenation process of Hb A. In order to gain full insight into the dynamic ensemble nature of the Hb molecule in solution and to correlate this feature with the functional properties of Hb, researchers need to develop novel techniques to obtain a quantitative description of the population distributions of various structures of unliganded (deoxy) and liganded (oxy and/or CO) forms as well as various partially liganded species under different experimental conditions. This is a challenging yet essential job for our eventual understanding not only of hemoglobin at the atomic and molecular level but also of other allosteric proteins.

## 6. CONCLUDING REMARKS

Hemoglobin has been a favorite molecule for researchers in biochemistry, biophysics, chemistry, computational biology, molecular biology, and structural biology. The structural determinations of Hb and Mb played a crucial role in establishing the field of structural biology. The classical two-structure description of Hb allostery pioneered by Perutz<sup>3</sup> in 1970, i.e., T  $\leftrightarrow$  R transition, has also evolved. Figure 16 is an illustration of an evolving view of Hb allostery. Figure 16a shows the superposition of the T and R structures of Hb, which allowed Perutz to propose his stereochemical mechanism for the cooperative oxygenation of Hb in 1970. The number of well-characterized T and R types of X-ray crystal structures of

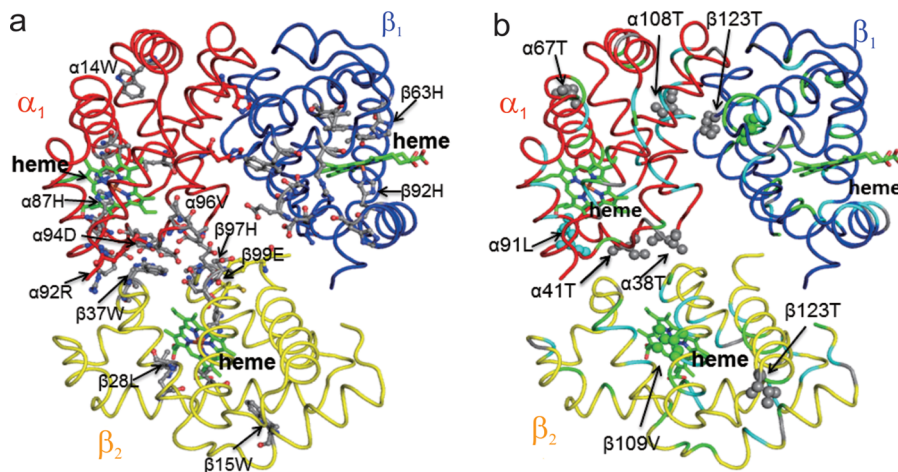


**Figure 17.** (a) Key amino acid residues in the  $\alpha_1\beta_1$  and  $\alpha_1\beta_2$  interfaces and the heme pockets of HbCO A.  $\alpha_2$  chain is not shown for clarity. (b) Locations of Val (blue), Leu (green), and Thr (gray) residues. Listed amino acid residues are likely to play important roles in transmitting signals during the cooperative oxygenation of Hb A. Figures were drawn according to coordinates under PDB code 2DN3. Figures were generated with the PyMOL program.<sup>61</sup>

Hb summarized in Table 1 as well as the results obtained by NMR structural and dynamic studies described in this review clearly illustrate that the picture for Hb allostery is more complex. Figure 16b shows a picture of HbCO A in solution, illustrating a collection of the 10 best solution structures of HbCO A with one each of the T- and R-type crystal structures superimposed. The solution structure of HbCO A indicates that there are considerable amounts of flexibility in this molecule. There is little doubt that we have learned a great deal about this protein, in terms of dynamics, function, and structure, during the past decade. The NMR structural and dynamic results presented in this review clearly show that there are various types of interactions among many amino acid residues in the deoxy and oxy (or carbonmonoxy) forms and that they contribute to the effects of allosteric effectors on the structural, dynamic, and functional properties of this molecule. The binding of a ligand like O<sub>2</sub> or CO as well as allosteric effectors to deoxy-Hb A can initiate various structural and dynamic changes (some might be subtle changes and some can cause large changes in conformations and thus alter the functional properties) in the molecule. Because of the complexity of the structural and dynamic changes in the Hb molecule upon oxygenation, it is a very challenging task to describe them in simple models, especially in a quantitative and statistical manner. Hence, it is not surprising that none of the models proposed for hemoglobin allostery can fully account for the details of cooperative oxygenation of Hb A and the effects of allosteric effectors on the function of Hb A. This is truly an irony in science, i.e., the more we know about a protein the less we are certain about its intimate details!

In order to gain an understanding of the atomic and molecular details of the cooperative oxygenation of Hb A, a new approach is needed making use of new techniques, e.g., NMR in combination with WAXS,<sup>84,178</sup> to monitor the structural and dynamic changes of the key amino acid residues of Hb A in the transition from the deoxy (unliganded) form to the oxy or CO (liganded) form as a function of the partial pressure of oxygen or carbon monoxide in the absence and presence of allosteric effectors. As mentioned earlier, WAXS has evolved during the past few years to become a powerful

technique for characterization of protein conformations and fluctuations in solution.

The results of multinuclear, multidimensional NMR experiments reported here give an idea of the possibilities available for future research. For example, our RDCs were measured only for the amide NHs, although RDCs can be measured also for other pairs of nuclei. Relaxation properties, dynamics, and its interplay with the structure for native as well as mutant Hbs can be investigated under a larger variety of experimental conditions in order to correlate them with the functional studies. Figure 17 is an illustration of some of the key amino acid residues (based on our studies) that can give important information on the allosteric pathways for Hb A during the oxygenation process. There are excellent NMR-based tertiary and quaternary structural markers of the Hb molecule to guide the experiments. The NMR markers are correlated not only with the structural changes upon ligation but also with the functional properties of Hb A as a function of pH, temperature, and allosteric effectors. In addition, one also has the potential to observe specific structural and dynamic changes of specific amino acid residues under different experimental conditions. From these experiments, one could gain some detailed structural and dynamic insights regarding the signaling pathways from one amino acid to the next as well as the relationship between tertiary and quaternary structural transitions during the oxygenation process. These are indeed very challenging experiments, but the results obtained will provide much needed information on the molecular basis of hemoglobin allostery. For example, we would like to know the relationship among the tertiary and quaternary structural changes and ligation state as well as the effects of allosteric effectors on the cooperative oxygenation process. These challenging as well as exciting experiments could provide information on the relationship between the tertiary and the quaternary changes on oxygenation, i.e., is the quaternary structural change concerted or sequential? This has been a much debated question in hemoglobin allostery. This approach can also be of value in designing new ways to understand other allosteric proteins in important cellular regulatory pathways.

## 1326 AUTHOR INFORMATION

## 1327 Corresponding Author

1328 \*E-mail: chienho@andrew.cmu.edu.

## 1329 Notes

1330 The authors declare no competing financial interest.

## 1331 Biographies



1332 Yue Yuan was Senior Research Biologist in the Department of  
 1333 Biological Sciences at Carnegie Mellon University, Pittsburgh, PA. She  
 1334 received her Ph.D. degree in Pharmaceutical Chemistry in 1995 from  
 1335 the Beijing Institute of Pharmacology and Toxicology under the  
 1336 guidance of Professor Kefang Jiao. She started working on protein  
 1337 NMR in 1995 at Beijing University with Professor Xiaocheng Gu. As a  
 1338 postdoctoral Fellow, she joined Professor Chien Ho's research group  
 1339 at Carnegie Mellon University in 1999 and then the group of Professor  
 1340 B. Mario Pinto at Simon Fraser University in Canada in 2003. She  
 1341 returned to Carnegie Mellon University with Professor Chien Ho in  
 1342 2008 as a Research Biologist. She is currently working as a Senior  
 1343 Scientist at the University of Notre Dame, IN. Her research interests  
 1344 are applications of NMR to study structure–function relationships of  
 1345 proteins.



1346 Ming F. Tam did his undergraduate work at the University of  
 1347 California, Davis, and received his B.S. degree in Chemistry in 1974.  
 1348 He then studied under Professor Walter E. Hill at the University of  
 1349 Montana and received his Ph.D. degree in 1981. He did postdoctoral  
 1350 research with Professor Masayasu Nomura at the Enzyme Institute of  
 1351 University of Wisconsin at Madison from 1982 to 1984. From 1984 to  
 1352 1986, he was a Research Scientist at Pharmacia Inc., designing  
 1353 instruments for liquid chromatography and DNA synthesis. From  
 1354 1986 to 2011, he was an Associate Research Fellow and then Research  
 1355 Fellow at the Institute of Molecular Biology, Academia Sinica, in  
 1356 Taiwan. He joined the Department of Biological Sciences at Carnegie

Mellon University as Senior Research Biologist in 2011. He is a 1357 protein chemist who has worked with glutathione S-transferases, 1358 arginine methyltransferases, and hemoglobin. His current interest is in 1359 elucidating the allosteric mechanism of hemoglobin oxygen binding. 1360



1361 Virgil Simplaceanu is NMR Spectroscopist in the Department of 1362 Biological Sciences at Carnegie Mellon University. He graduated from 1362 the Polytechnical Institute in Bucharest, Romania, in 1969 as an 1363 electronics engineer with a specialty in technical physics and then 1364 worked as a Research Associate at the Institute for Atomic Physics in 1365 Magurele, Bucharest, Romania, in the NMR laboratory of Professor 1366 Ioan Ursu. Since 1981 he has worked with Professor Chien Ho at 1367 Carnegie Mellon University, and his interests are NMR instrumenta- 1368 tion and applications of NMR to biology and chemistry. 1369



1370 Chien Ho did his undergraduate training at Williams College and 1370 received his B.A. degree in Chemistry in 1957. He then went to Yale 1371 University for graduate work in physical chemistry with Julian M. 1372 Sturtevant and received his Ph.D. degree in 1961. From 1960 to 1961, 1373 he was a Research Chemist for Linde Co., Union Carbide Corp., 1374 working on the liquid nitrogen temperature preservation of human 1375 blood. From 1961 to 1964, he did postdoctoral research with George 1376 Scatchard and Jancinto Steinhardt in the Department of Chemistry 1377 and with David F. Waugh in the Department of Biology, 1378 Massachusetts Institute of Technology. From 1964 to 1979, he was 1379 an assistant professor, associate professor, and professor of molecular 1380 biology at the University of Pittsburgh. In 1979, he joined Carnegie 1381 Mellon University as the head and professor of the Department of 1382 Biological Sciences. Since 1985, he is Alumni Professor of Biological 1383 Sciences at Carnegie Mellon University. His research goal is to 1384 understand the relationship between the structure and function in 1385 biological systems by correlating information obtained from 1386 biochemical, biophysical, and molecular biological techniques. His 1387 current research is focused in two areas. The first centers on a study of 1388 human normal and abnormal hemoglobins in order to correlate the 1389

1390 structure, dynamics, and function of hemoglobin in solution. He  
 1391 received a MERIT Award in 1986 from the National Heart, Lung, and  
 1392 Blood Institute for his research on hemoglobin. The second centers on  
 1393 the application of magnetic resonance imaging (MRI) and spectroscopy  
 1394 (MRS) to biomedical systems. He is currently developing  
 1395 noninvasive techniques to monitor the migration/accumulation of  
 1396 immune cells in vivo by MRI as a means to detect early signs of graft  
 1397 rejection following solid organ transplantation.

## 1398 ACKNOWLEDGMENTS

1399 We thank the National Institutes of Health for support of our  
 1400 research on hemoglobin (R01GM084614). We also thank Drs.  
 1401 William A. Eaton, Martin Karplus, Lee Makowski, John S.  
 1402 Olson, E. Ann Pratt, Gordon Rule, and Nico Tjandra for  
 1403 helpful comments and suggestions to improve our manuscript.

## 1404 ABBREVIATIONS

1405 Hb	hemoglobin
1406 Hb A	human normal adult hemoglobin
1407 HbCO	carbonmonoxy-hemoglobin
1408 deoxy-Hb	deoxy-hemoglobin
1409 met-Hb	methemoglobin
1410 rHb	recombinant hemoglobin
1411 Mb	myoglobin
1412 T structure	tense structure
1413 R structure	relaxed structure
1414 HEPES	N-(2-hydroxyethyl)-piperazine-N'-2-ethanesulfonic acid
1415 PEG	polyethylene glycol
1416 IHP	inositol hexaphosphate
1417 2,3-BPG	2,3-bisphosphoglycerate
1418 KNF	Koshland, Nemethy, Filmer
1419 MWC	Monod, Wyman, Changeux
1420 NMR	nuclear magnetic resonance
1421 PDB	Protein Data Bank
1422 $R_1$	longitudinal relaxation rate
1423 $R_2$	transverse relaxation rate
1424 $S^2$	generalized order parameter
1425 $S_{\text{axis}}^2$	order parameter for the methyl rotation axis
1426 $R_{\text{ex}}$	conformational exchange contribution to transverse relaxation rate
1427 RCSB	Research Collaboratory Structural Bioinformatics
1428 RDC	residual dipolar coupling
1429 HSQC	heteronuclear single-quantum coherence
1430 TROSY	transverse relaxation-optimized spectroscopy
1431 RMSD	root-mean-square deviation
1432 WAXS	wide-angle X-ray scattering
1433 $J_{\text{HN}}$	scalar coupling between H and N of the amide group
1434 $D_{\text{HN}}$	dipolar coupling
1435 $k_{\text{ox}}$	autoxidation rate constant
1436 $k_{\text{az}}$	azide-induced autoxidation rate constant

## 1438 REFERENCES

- 1439 (1) Dickerson, R. E.; Geis, I. *Hemoglobin: Structure, Function, Evolution, and Pathology*; Benjamin/Cummings: Menlo Park, CA, 1983.
- 1440 (2) Monod, J.; Wyman, J.; Changeux, J. P. *J. Mol. Biol.* **1965**, *12*, 88.
- 1441 (3) Perutz, M. F. *Nature* **1970**, *228*, 726.
- 1442 (4) Koshland, D. E., Jr. *J. Cell. Comp. Physiol.* **1959**, *54*, 245.
- 1443 (5) Koshland, D. E., Jr.; Nemethy, G.; Filmer, D. *Biochemistry* **1966**, *5*, 365.
- 1444 (6) Szabo, A.; Karplus, M. *J. Mol. Biol.* **1972**, *72*, 163.
- (7) Lee, A. W.; Karplus, M. *Proc. Natl. Acad. Sci. U.S.A.* **1983**, *80*, 1448 7055.
- (8) Yonetani, T.; Park, S.; Tsuneshige, A.; Imai, K.; Kanaori, K. *J. Biol. Chem.* **2002**, *277*, 34508.
- (9) Henry, E. R.; Bettati, S.; Hofrichter, J.; Eaton, W. A. *Biophys. Chem.* **2002**, *98*, 149.
- (10) Ackers, G. K.; Doyle, M. L.; Myers, D.; Daugherty, M. A. *Science* **1992**, *255*, 54.
- (11) Ackers, G. K. *Adv. Protein Chem.* **1998**, *51*, 185.
- (12) Lukin, J. A.; Ho, C. *Chem. Rev.* **2004**, *104*, 1219.
- (13) Hopfield, J. J. *J. Mol. Biol.* **1973**, *77*, 207.
- (14) Shulman, R. G.; Hopfield, J. J.; Ogawa, S. *Q. Rev. Biophys.* **1975**, *8*, 325.
- (15) Perutz, M. F.; Wilkinson, A. J.; Paoli, M.; Dodson, G. G. *Annu. Rev. Biophys. Biomol. Struct.* **1998**, *27*, 1.
- (16) Eaton, W. A.; Henry, E. R.; Hofrichter, J.; Mozzarelli, A. *Nat. Struct. Biol.* **1999**, *6*, 351.
- (17) Shibayama, N. *J. Mol. Biol.* **1999**, *285*, 1383.
- (18) Ackers, G. K.; Holt, J. M.; Huang, Y.; Grinkova, Y.; Klinger, A.; Denisov, I. *Proteins* **2000**, *Suppl 4*, 23.
- (19) Shulman, R. G. *IUBMB Life* **2001**, *51*, 351.
- (20) Yun, K. M.; Morimoto, H.; Shibayama, N. *J. Biol. Chem.* **2002**, *277*, 1878.
- (21) Yonetani, T.; Laberge, M. *Biochim. Biophys. Acta* **2008**, *1784*, 1146.
- (22) Safo, M.; Ahmed, M.; Ghadge, M.; Boyiri, T. *Biochim. Biophys. Acta* **2011**, *1814*, 797.
- (23) Belletti, A.; Brunori, M. *Biochim. Biophys. Acta* **2011**, *1807*, 1262.
- (24) Changeux, J. P.; Edelstein, S. *F1000 Biol. Rep.* **2011**, *3*, 19.
- (25) Changeux, J.-P. *Annu. Rev. Biophys.* **2012**, *41*, 103.
- (26) Jones, E. M.; Balakrishnan, G.; Spiro, T. G. *J. Am. Chem. Soc.* **2012**, *134*, 3461.
- (27) Yonetani, T.; Kanaori, K. *Biochim. Biophys. Acta* **2013**, *1834*, 1873.
- (28) Tekpinar, M.; Zheng, W. *Proteins* **2013**, *81*, 240.
- (29) Brunori, M. *FEBS J.* **2014**, *281*, 633.
- (30) Jones, E. M.; Monza, E.; Balakrishnan, G.; Blouin, G. C.; Mak, P.; Zhu, Q.; Kincaid, J. R.; Guallar, V.; Spiro, T. G. *J. Am. Chem. Soc.* **2014**, *136*, 10325.
- (31) Viappiani, C.; Abbruzzetti, S.; Ronda, L.; Bettati, S.; Henry, E.; Mozzarelli, A.; Eaton, W. A. *Proc. Natl. Acad. Sci. U.S.A.* **2014**, *111*, 12758.
- (32) Baldwin, J.; Chothia, C. *J. Mol. Biol.* **1979**, *129*, 175.
- (33) Perutz, M. F. *Brookhaven Symp. Biol.* **1960**, *13*, 165.
- (34) Muirhead, H.; Perutz, M. F. *Nature* **1963**, *199*, 633.
- (35) Park, S.-Y.; Yokoyama, T.; Shibayama, N.; Shiro, Y.; Tame, J. R. *H. J. Mol. Biol.* **2006**, *360*, 690.
- (36) Savino, C.; Miele, A. E.; Draghi, F.; Johnson, K. A.; Sciaro, G.; Brunori, M.; Vallone, B. *Biopolymers* **2009**, *91*, 1097.
- (37) Perutz, M. F. *J. Cryst. Growth* **1968**, *2*, 54.
- (38) Abassi, Z.; Kotob, S.; Pieruzzi, F.; Abouassali, M.; Keiser, H. R.; Fratantoni, J. C.; Alayash, A. I. *J. Lab. Clin. Med.* **1997**, *129*, 603.
- (39) Vasquez, G. B.; Ji, X. H.; Fronticelli, C.; Gilliland, G. L. *Acta Crystallogr., Sect. D: Biol. Crystallogr.* **1998**, *54*, 355.
- (40) Derewenda, Z.; Dodson, G.; Emsley, P.; Harris, D.; Nagai, K.; Perutz, M.; Reynaud, J. P. *J. Mol. Biol.* **1990**, *211*, 515.
- (41) Fermi, G. *J. Mol. Biol.* **1975**, *97*, 237.
- (42) Fermi, G.; Perutz, M. F.; Shaanan, B.; Fourme, R. *J. Mol. Biol.* **1984**, *175*, 159.
- (43) Pechik, I.; Ji, X.; Fidelis, K.; Karavitis, M.; Moult, J.; Brinigar, W.; Fronticelli, C.; Gilliland, G. L. *Biochemistry* **1996**, *35*, 1935.
- (44) Safo, M. K.; Burnett, J. C.; Musayev, F. N.; Nokuri, S.; Abraham, D. J. *Acta Crystallogr., Sect. D: Biol. Crystallogr.* **2002**, *58*, 2031.
- (45) Shaanan, B. *J. Mol. Biol.* **1983**, *171*, 31.
- (46) Tame, J. R. H.; Vallone, B. *Acta Crystallogr., Sect. D: Biol. Crystallogr.* **2000**, *56*, 805.
- (47) Silva, M. M.; Rogers, P. H.; Arnone, A. J. *Biol. Chem.* **1992**, *267*, 17248.

- 1516 (48) Mueser, T. C.; Rogers, P. H.; Arnone, A. *Biochemistry* **2000**, *39*,  
1517 15353.
- 1518 (49) Srinivasan, R.; Rose, G. D. *Proc. Natl. Acad. Sci. U.S.A.* **1994**, *91*,  
1519 11113.
- 1520 (50) Janin, J.; Wodak, S. J. *Proteins* **1993**, *15*, 1.
- 1521 (51) Smith, F. R.; Lattman, E. E.; Carter, C. W. *Proteins* **1991**, *10*, 81.
- 1522 (52) Smith, F. R.; Simmons, K. C. *Proteins* **1994**, *18*, 295.
- 1523 (53) Safo, M. K.; Abraham, D. J. *Biochemistry* **2005**, *44*, 8347.
- 1524 (54) Jenkins, J. D.; Musayev, F. N.; Danso-Danquah, R.; Abraham, D.  
1525 J.; Safo, M. K. *Acta Crystallogr., Sect. D: Biol. Crystallogr.* **2009**, *65*, 41.
- 1526 (55) Kavanaugh, J. S.; Rogers, P. H.; Arnone, A. *Biochemistry* **2005**,  
1527 *44*, 6101.
- 1528 (56) Liddington, R.; Derewenda, Z.; Dodson, E.; Hubbard, R.;  
1529 Dodson, G. *J. Mol. Biol.* **1992**, *228*, 551.
- 1530 (57) Richard, V.; Dodson, G. G.; Mauguen, Y. *J. Mol. Biol.* **1993**, *233*,  
1531 270.
- 1532 (58) Dodson, G. G.; Richard, V. R.; Tolley, S. P.; Waller, D. A.;  
1533 Weber, R. E. *J. Mol. Biol.* **1990**, *211*, 691.
- 1534 (59) Yokoyama, T.; Neya, S.; Tsuneshige, A.; Yonetani, T.; Park, S.  
1535 Y.; Tame, J. R. H. *J. Mol. Biol.* **2006**, *356*, 790.
- 1536 (60) Shibayama, N.; Sugiyama, K.; Tame, J. R.; Park, S. Y. *J. Am.*  
1537 *Chem. Soc.* **2014**, *136*, 5097.
- 1538 (61) DeLano, W. L. *The PyMOL Molecular Graphics System*, Version  
1539 1.5.0.4; Schrodinger, LLC.: Palo Alto, CA, 2002.
- 1540 (62) Kavanaugh, J. S.; Weydert, J. A.; Rogers, P. H.; Arnone, A.  
1541 *Biochemistry* **1998**, *37*, 4358.
- 1542 (63) Dey, S.; Chakrabarti, P.; Janin, J. *Proteins* **2011**, *79*, 2861.
- 1543 (64) Seixas, F. A. V.; de Azevedo, W. F.; Colombo, M. F. *Acta*  
1544 *Crystallogr., Sect. D: Biol. Crystallogr.* **1999**, *55*, 1914.
- 1545 (65) Chan, N. L.; Kavanaugh, J. S.; Rogers, P. H.; Arnone, A.  
1546 *Biochemistry* **2004**, *43*, 118.
- 1547 (66) Kavanaugh, J. S.; Moopenn, W. F.; Arnone, A. *Biochemistry*  
1548 **1993**, *32*, 2509.
- 1549 (67) Shen, T. J.; Ho, N. T.; Simplaceanu, V.; Zou, M.; Green, B. N.;  
1550 Tam, M. F.; Ho, C. *Proc. Natl. Acad. Sci. U.S.A.* **1993**, *90*, 8108.
- 1551 (68) Simplaceanu, V.; Lukin, J. A.; Fang, T. Y.; Zou, M.; Ho, N. T.;  
1552 Ho, C. *Biophys. J.* **2000**, *79*, 1146.
- 1553 (69) Lukin, J. A.; Kontaxis, G.; Simplaceanu, V.; Yuan, Y.; Bax, A.;  
1554 Ho, C. *Proc. Natl. Acad. Sci. U.S.A.* **2003**, *100*, 517.
- 1555 (70) Gong, Q. G.; Simplaceanu, V.; Lukin, J. A.; Giovannelli, J. L.;  
1556 Ho, N. T.; Ho, C. *Biochemistry* **2006**, *45*, 5140.
- 1557 (71) Sahu, S. C.; Simplaceanu, V.; Gong, Q. G.; Ho, N. T.; Glushka,  
1558 J. G.; Prestegard, J. H.; Ho, C. *J. Am. Chem. Soc.* **2006**, *128*, 6290.
- 1559 (72) Sahu, S. C.; Simplaceanu, V.; Gong, Q.; Ho, N. T.; Tian, F.;  
1560 Prestegard, J. H.; Ho, C. *Biochemistry* **2007**, *46*, 9973.
- 1561 (73) Ho, C.; Yuan, Y.; Simplaceanu, V. In *Hemoglobin: Recent*  
1562 *Developments and Topics*; Nagai, M., Ed.; Research Signpost: Kerala,  
1563 India, 2011.
- 1564 (74) Fan, J. S.; Zheng, Y.; Choy, W. Y.; Simplaceanu, V.; Ho, N. T.;  
1565 Ho, C.; Yang, D. *Biochemistry* **2013**, *52*, 5809.
- 1566 (75) Tjandra, N.; Bax, A. *Science* **1997**, *278*, 1697.
- 1567 (76) Xu, Y.; Zheng, Y.; Fan, J.-S.; Yang, D. *Nat. Methods* **2006**, *3*, 931.
- 1568 (77) Arnone, A. *Nature* **1972**, *237*, 146.
- 1569 (78) Arnone, A.; Perutz, M. F. *Nature* **1974**, *249*, 34.
- 1570 (79) Zuiderweg, E. R.; Hamers, L. F.; de Bruin, S. H.; Hilbers, C. W.  
1571 *Eur. J. Biochem.* **1981**, *118*, 85.
- 1572 (80) Nagatomo, S.; Nagai, M.; Mizutani, Y.; Yonetani, T.; Kitagawa,  
1573 T. *Biophys. J.* **2005**, *89*, 1203.
- 1574 (81) Song, X. J.; Yuan, Y.; Simplaceanu, V.; Sahu, S. C.; Ho, N. T.;  
1575 Ho, C. *Biochemistry* **2007**, *46*, 6795.
- 1576 (82) Park, S.; Bardhan, J. P.; Roux, B.; Makowski, L. *J. Chem. Phys.*  
1577 **2009**, *130*, 134114.
- 1578 (83) Makowski, L.; Rodi, D. J.; Mandava, S.; Minh, D. D.; Gore, D.  
1579 B.; Fischetti, R. F. *J. Mol. Biol.* **2008**, *375*, 529.
- 1580 (84) Makowski, L.; Bardhan, J.; Gore, D.; Lal, J.; Mandava, S.; Park,  
1581 S.; Rodi, D. J.; Ho, N. T.; Ho, C.; Fischetti, R. F. *J. Mol. Biol.* **2011**,  
1582 *408*, 909.
- 1583 (85) Makowski, L.; Gore, D.; Mandava, S.; Minh, D.; Park, S.; Rodi,  
1584 D. J.; Fischetti, R. F. *Biopolymers* **2011**, *95*, 531.
- (86) Tsai, C. H.; Shen, T. J.; Ho, N. T.; Ho, C. *Biochemistry* **1999**, *38*, 1585  
8751.
- (87) Mihailescu, M. R.; Russu, I. M. *Proc. Natl. Acad. Sci. U.S.A.* **2001**, 1586  
98, 3773.
- (88) Lukin, J. A.; Kontaxis, G.; Simplaceanu, V.; Yuan, Y.; Bax, A.;  
Ho, C. *J. Biomol. NMR* **2004**, *28*, 203.
- (89) Sahu, S. C.; Simplaceanu, V.; Ho, N. T.; Giovannelli, J. L.; Ho, C. *J. Biomol. NMR* **2006**, *36*, 1.
- (90) Song, X. J.; Simplaceanu, V.; Ho, N. T.; Ho, C. *Biochemistry* **2008**, *47*, 4907.
- (91) Mandel, A. M.; Akke, M.; Palmer, A. G. *J. Mol. Biol.* **1995**, *246*, 1595  
144.
- (92) Wang, C. Y.; Rance, M.; Palmer, A. G. *J. Am. Chem. Soc.* **2003**, 1597  
125, 8968.
- (93) Loria, J. P.; Rance, M.; Palmer, A. G. *J. Am. Chem. Soc.* **1999**, 1599  
121, 2331.
- (94) Millet, O.; Loria, J. P.; Kroenke, C. D.; Pons, M.; Palmer, A. G. *J. Am. Chem. Soc.* **2000**, *122*, 2867.
- (95) Yuan, Y.; Simplaceanu, V.; Lukin, J. A.; Ho, C. *J. Mol. Biol.* **2002**, 1603  
321, 863.
- (96) Balakrishnan, G.; Tsai, C. H.; Wu, Q.; Case, M. A.; Pevsner, A.;  
McLendon, G. L.; Ho, C.; Spiro, T. G. *J. Mol. Biol.* **2004**, *340*, 857.
- (97) Balakrishnan, G.; Case, M. A.; Pevsner, A.; Zhao, X. J.;  
Tengroth, C.; McLendon, G. L.; Spiro, T. G. *J. Mol. Biol.* **2004**, *340*, 1608  
843.
- (98) Yang, D. W.; Mittermaier, A.; Mok, Y. K.; Kay, L. E. *J. Mol. Biol.* **1998**, *276*, 939.
- (99) Zuiderweg, E. R.; Hamers, L. F.; Rollema, H. S.; de Bruin, S. H.;  
Hilbers, C. W. *Eur. J. Biochem.* **1981**, *118*, 95.
- (100) Hwang, T. L.; van Zijl, P. C. M.; Mori, S. *J. Biomol. NMR* **1998**, *11*, 221.
- (101) Bunn, H. F.; Forget, B. G. *Hemoglobin: molecular, genetic and*  
1616 *clinical aspects*; W.B. Saunders: Philadelphia, PA, 1986.
- (102) Wyman, J. *Adv. Protein Chem.* **1964**, *19*, 223.
- (103) Ho, C.; Yuan, Y. In *Encyclopedia of Life Sciences*; John Wiley &  
1619 Sons, Ltd.: Chichester, 2010.
- (104) Perutz, M. F. *Nature* **1970**, *228*, 734.
- (105) Busch, M. R.; Ho, C. *Biophys. Chem.* **1990**, *37*, 313.
- (106) Busch, M. R.; Mace, J. E.; Ho, N. T.; Ho, C. *Biochemistry* **1991**, 1623  
30, 1865.
- (107) Sun, D. Z. P.; Zou, M.; Ho, N. T.; Ho, C. *Biochemistry* **1997**, *36*, 6663.
- (108) Fang, T. Y.; Zou, M.; Simplaceanu, V.; Ho, N. T.; Ho, C. *Biochemistry* **1999**, *38*, 13423.
- (109) Kilmartin, J. V.; Rossi-Bernardi, L. *Nature* **1969**, *222*, 1243.
- (110) Zheng, G.; Schaefer, M.; Karplus, M. *Biochemistry* **2013**, *52*, 1630  
8539.
- (111) Russu, I. M.; Ho, N. T.; Ho, C. *Biochemistry* **1980**, *19*, 1043.
- (112) Perutz, M. F.; Kilmartin, J. V.; Nishikura, K.; Fogg, J. H.;  
Butler, P. J. G.; Rollema, H. S. *J. Mol. Biol.* **1980**, *138*, 649.
- (113) Kilmartin, J. V.; Fogg, J. H.; Perutz, M. F. *Biochemistry* **1980**, 1635  
19, 3189.
- (114) Perutz, M. F.; Gronenborn, A. M.; Clore, G. M.; Shih, D. T.;  
Craescu, C. T. *J. Mol. Biol.* **1985**, *186*, 471.
- (115) Perutz, M. F.; Gronenborn, A. M.; Clore, G. M.; Fogg, J. H.;  
Shih, D. T. B. *J. Mol. Biol.* **1985**, *183*, 491.
- (116) Russu, I. M.; Ho, C. *Biochemistry* **1986**, *25*, 1706.
- (117) Ho, C.; Russu, I. M. *Biochemistry* **1987**, *26*, 6299.
- (118) Shih, D. T. B.; Perutz, M. F. *J. Mol. Biol.* **1987**, *195*, 419.
- (119) Shih, D. T. B.; Perutz, M. F.; Gronenborn, A. M.; Clore, G. M.  
*J. Mol. Biol.* **1987**, *195*, 453.
- (120) Russu, I. M.; Wu, S. S.; Ho, N. T.; Kellogg, G. W.; Ho, C.  
*Biochemistry* **1989**, *28*, 5298.
- (121) Campbell, K. L.; Roberts, J. E. E.; Watson, L. N.; Stetefeld, J.;  
Sloan, A. M.; Signore, A. V.; Howatt, J. W.; Tame, J. R. H.; Rohland,  
N.; Shen, T. J.; Austin, J. J.; Hofreiter, M.; Ho, C.; Weber, R. E.;  
Cooper, A. *Nat. Genet.* **2010**, *42*, 536.

- 1652 (122) Yuan, Y.; Shen, T. J.; Gupta, P.; Ho, N. T.; Simplaceanu, V.;  
1653 Tam, T. C.; Hofreiter, M.; Cooper, A.; Campbell, K. L.; Ho, C.  
1654 *Biochemistry* **2011**, *50*, 7350.
- 1655 (123) Yuan, Y.; Byrd, C.; Shen, T.-J.; Simplaceanu, V.; Tam, T. C. S.;  
1656 Ho, C. *Biochemistry* **2013**, *52*, 8888.
- 1657 (124) Shih, D. T.; Jones, R. T.; Imai, K.; Tyuma, I. *J. Biol. Chem.*  
1658 **1985**, *260*, 5919.
- 1659 (125) Noguchi, H.; Campbell, K. L.; Ho, C.; Unzai, S.; Park, S. Y.;  
1660 Tame, J. R. *Acta Crystallogr., Sect. D: Biol. Crystallogr.* **2012**, *68*, 1441.
- 1661 (126) Kavanaugh, J. S.; Rogers, P. H.; Arnone, A. *Biochemistry* **1992**,  
1662 *31*, 8640.
- 1663 (127) Perutz, M. F.; Fermi, G.; Poyart, C.; Pagnier, J.; Kister, J. *J. Mol.*  
1664 *Biol.* **1993**, *233*, 536.
- 1665 (128) Yonetani, T.; Yamamoto, H.; Iizuka, T. *J. Biol. Chem.* **1974**,  
1666 *249*, 2168.
- 1667 (129) Kitagawa, T.; Ondrias, M. R.; Rousseau, D. L.; Ikeda-Saito, M.;  
1668 Yonetani, T. *Nature* **1982**, *298*, 869.
- 1669 (130) Lukin, J. A.; Simplaceanu, V.; Zou, M.; Ho, N. T.; Ho, C. *Proc.*  
1670 *Natl. Acad. Sci. U.S.A.* **2000**, *97*, 10354.
- 1671 (131) Yuan, Y.; Simplaceanu, V.; Ho, N. T.; Ho, C. *Biochemistry*  
1672 **2010**, *49*, 10606.
- 1673 (132) Birukou, I.; Schweers, R. L.; Olson, J. S. *J. Biol. Chem.* **2010**,  
1674 *285*, 8840.
- 1675 (133) Birukou, I.; Maillett, D. H.; Birukova, A.; Olson, J. S.  
1676 *Biochemistry* **2011**, *50*, 7361.
- 1677 (134) Eich, R. F.; Li, T.; Lemon, D. D.; Doherty, D. H.; Curry, S. R.;  
1678 Aitken, J. F.; Mathews, A. J.; Johnson, K. A.; Smith, R. D.; Phillips, G.  
1679 N., Jr.; Olson, J. S. *Biochemistry* **1996**, *35*, 6976.
- 1680 (135) Fronticelli, C.; Brinigar, W. S.; Olson, J. S.; Bucci, E.;  
1681 Gryczynski, Z.; O'Donnell, J. K.; Kowalczyk, J. *Biochemistry* **1993**, *32*,  
1682 1235.
- 1683 (136) Jeong, S. T.; Ho, N. T.; Hendrich, M. P.; Ho, C. *Biochemistry*  
1684 **1999**, *38*, 13433.
- 1685 (137) Karavitis, M.; Fronticelli, C.; Brinigar, W. S.; Vasquez, G. B.;  
1686 Militello, V.; Leone, M.; Cupane, A. *J. Biol. Chem.* **1998**, *273*, 23740.
- 1687 (138) Maillett, D. H.; Simplaceanu, V.; Shen, T. J.; Ho, N. T.; Olson,  
1688 J. S.; Ho, C. *Biochemistry* **2008**, *47*, 10551.
- 1689 (139) Mathews, A. J.; Olson, J. S.; Renaud, J. P.; Tame, J.; Nagai, K. J.  
1690 *Biol. Chem.* **1991**, *266*, 21631.
- 1691 (140) Mathews, A. J.; Rohlf, R. J.; Olson, J. S.; Tame, J.; Renaud, J.  
1692 P.; Nagai, K. *J. Biol. Chem.* **1989**, *264*, 16573.
- 1693 (141) Nagai, K.; Luisi, B.; Shih, D.; Miyazaki, G.; Imai, K.; Poyart, C.;  
1694 De Young, A.; Kwiatkowski, L.; Noble, R. W.; Lin, S. H.; Yu, N. T.  
1695 *Nature* **1987**, *329*, 858.
- 1696 (142) Tam, M. F.; Rice, N. W.; Maillett, D. H.; Simplaceanu, V.; Ho,  
1697 N. T.; Tam, T. C.; Shen, T. J.; Ho, C. *J. Biol. Chem.* **2013**, *288*, 25512.
- 1698 (143) Tucker, P. W.; Phillips, S. E. V.; Perutz, M. F.; Houtchens, R.;  
1699 Caughey, W. S. *Proc. Natl. Acad. Sci. U.S.A.* **1978**, *75*, 1076.
- 1700 (144) Tsuruga, M.; Shikama, K. *Biochim. Biophys. Acta* **1997**, *1337*,  
1701 96.
- 1702 (145) Macdonald, V. W. In *Methods Enzymol.*; Academic Press Inc.:  
1703 San Diego, 1994; Vol. 231, p 480.
- 1704 (146) Brancaccio, A.; Cutruzzola, F.; Allocatelli, C.; Brunori, M.;  
1705 Smerdon, S.; Wilkinson, A.; Dou, Y.; Keenan, D.; Ikeda-Saito, M.;  
1706 Brantley, R., Jr. *J. Biol. Chem.* **1994**, *269*, 13843.
- 1707 (147) Brantley, R. E., Jr.; Smerdon, S. J.; Wilkinson, A. J.; Singleton,  
1708 E. W.; Olson, J. S. *J. Biol. Chem.* **1993**, *268*, 6995.
- 1709 (148) Carver, T. E.; Brantley, R. E., Jr.; Singleton, E. W.; Arduini, R.  
1710 M.; Quillin, M. L.; Phillips, G. N., Jr.; Olson, J. S. *J. Biol. Chem.* **1992**,  
1711 *267*, 14443.
- 1712 (149) Quillin, M. L.; Li, T.; Olson, J. S.; Phillips, G. N., Jr.; Dou, Y.;  
1713 Ikeda-Saito, M.; Regan, R.; Carlson, M.; Gibson, Q. H.; Li, H.; et al. *J.*  
1714 *Mol. Biol.* **1995**, *245*, 416.
- 1715 (150) Wallace, W. J.; Houtchens, R. A.; Maxwell, J. C.; Caughey, W.  
1716 *S. J. Biol. Chem.* **1982**, *257*, 4966.
- 1717 (151) Suzuki, T.; Watanabe, Y. H.; Nagasawa, M.; Matsuoka, A.;  
1718 Shikama, K. *Eur. J. Biochem.* **2000**, *267*, 6166.
- 1719 (152) Tsuruga, M.; Matsuoka, A.; Hachimori, A.; Sugawara, Y.;  
1720 Shikama, K. *J. Biol. Chem.* **1998**, *273*, 8607.
- 153 (153) Wiltrot, M. E.; Giovannelli, J. L.; Simplaceanu, V.; Lukin, J. 1721  
A.; Ho, N. T.; Ho, C. *Biochemistry* **2005**, *44*, 7207. 1722
- (154) Mansouri, A.; Winterhalter, K. H. *Biochemistry* **1973**, *12*, 4946. 1723
- (155) Tsai, C. H.; Fang, T. Y.; Ho, N. T.; Ho, C. *Biochemistry* **2000**, 1724  
39, 13719. 1725
- (156) Kim, H. W.; Shen, T. J.; Sun, D. P.; Ho, N. T.; Madrid, M.; Ho, 1726  
*C. J. Mol. Biol.* **1995**, *248*, 867. 1727
- (157) Tsai, C. H.; Ho, C. *Biophys. Chem.* **2002**, *98*, 15. 1728
- (158) Kern, D.; Zuiderweg, E. R. P. *Curr. Opin. Struct. Biol.* **2003**, *13*, 1729  
748. 1730
- (159) Tang, C.; Schwieters, C. D.; Clore, G. M. *Nature* **2007**, *449*, 1731  
1078. 1732
- (160) Eaton, W. A.; Henry, E. R.; Hofrichter, J.; Bettati, S.; Viappiani, 1733  
C.; Mozzarelli, A. *IUBMB Life* **2007**, *59*, 586. 1734
- (161) Velyvis, A.; Yang, Y. R.; Schachman, H. K.; Kay, L. E. *Proc.* 1735  
*Natl. Acad. Sci. U.S.A.* **2007**, *104*, 8815. 1736
- (162) Cui, Q.; Karplus, M. *Protein Sci.* **2008**, *17*, 1295. 1737
- (163) Lakomek, N. A.; Walter, K. F. A.; Fares, C.; Lange, O. F.; de 1738  
Groot, B. L.; Grubmuller, H.; Bruschweiler, R.; Munk, A.; Becker, S.; 1739  
Meiler, J.; Griesinger, C. *J. Biomol. NMR* **2008**, *41*, 139. 1740
- (164) Boehr, D. D.; Nussinov, R.; Wright, P. E. *Nat. Chem. Biol.* 1741  
**2009**, *5*, 789. 1742
- (165) Gua, Y.; Shrivastava, I. H.; Amara, S. G.; Bahar, I. *Proc. Natl.* 1743  
*Acad. Sci. U.S.A.* **2009**, *106*, 2589. 1744
- (166) Velyvis, A.; Schachman, H. K.; Kay, L. E. *J. Mol. Biol.* **2009**, 1745  
387, 540. 1746
- (167) Motlagh, H. N.; Wrabl, J. O.; Li, J.; Hilser, V. J. *Nature* **2014**, 1747  
508, 331. 1748
- (168) Fung, L. W. M.; Minton, A. P.; Lindstrom, T. R.; Pisciotta, A. 1749  
V.; Ho, C. *Biochemistry* **1977**, *16*, 1452. 1750
- (169) Takahashi, S.; Lin, A.; Ho, C. *Biochemistry* **1980**, *19*, 5196. 1751
- (170) Miura, S.; Ho, C. *Biochemistry* **1982**, *21*, 6280. 1752
- (171) Russu, I. M.; Ho, N. T.; Ho, C. *Biochim. Biophys. Acta* **1987**, 1753  
914, 40. 1754
- (172) Kim, H. W.; Shen, T. J.; Sun, D. P.; Ho, N. T.; Madrid, M.; 1755  
Tam, M. F.; Zou, M.; Cottam, P. F.; Ho, C. *Proc. Natl. Acad. Sci. U.S.A.* 1756  
**1994**, *91*, 11547. 1757
- (173) Barrick, D.; Ho, N. T.; Simplaceanu, V.; Dahlquist, F. W.; Ho, 1758  
*C. Nat. Struct. Biol.* **1997**, *4*, 78. 1759
- (174) Barrick, D.; Ho, N. T.; Simplaceanu, V.; Ho, C. *Biochemistry* **1997**, 1760  
*40*, 3780. 1761
- (175) Chang, C. K.; Simplaceanu, V.; Ho, C. *Biochemistry* **2002**, *41*, 1762  
5644. 1763
- (176) Kneipp, J.; Balakrishnan, G.; Chen, R. P.; Shen, T. J.; Sahu, S. 1764  
C.; Ho, N. T.; Giovannelli, J. L.; Simplaceanu, V.; Ho, C.; Spiro, T. G. 1765  
*J. Mol. Biol.* **2006**, *356*, 335. 1766
- (177) Petrich, J. W.; Lambry, J. C.; Kuczera, K.; Karplus, M.; Poyart, 1767  
C.; Martin, J. L. *Biochemistry* **1991**, *30*, 3975. 1768
- (178) Cammarata, M.; Levantino, M.; Wulff, M.; Cupane, A. *J. Mol.* 1769  
*Biol.* **2010**, *400*, 951. 1770
- (179) Cornilescu, G.; Marquardt, J. L.; Ottiger, M.; Bax, A. *J. Am.* 1771  
*Chem. Soc.* **1998**, *120*, 6836. 1772
- (180) Bax, A.; Kontaxis, G.; Tjandra, N. In *Methods in Enzymology*; 1773  
Academic Press Inc.: San Diego, 2001; Vol. 339, p 127. 1774